

LABCAT: Locally adaptive Bayesian optimization using principal component-aligned trust regions

E. Visser^{a,*}, C.E. van Daalen^a, J.C. Schoeman^a

^a*Department of Electrical and Electronic Engineering, Stellenbosch University, South Africa*

Abstract

Bayesian optimization (BO) is a popular method for optimizing expensive black-box functions. BO has several well-documented shortcomings, including computational slowdown with longer optimization runs, poor suitability for non-stationary or ill-conditioned objective functions, and poor convergence characteristics. Several algorithms have been proposed that incorporate local strategies, such as trust regions, into BO to mitigate these limitations; however, none address all of them satisfactorily. To address these shortcomings, we propose the LABCAT algorithm, which extends trust-region-based BO by adding principal-component-aligned rotation and an adaptive rescaling strategy based on the length-scales of a local Gaussian process surrogate model with automatic relevance determination. Through extensive numerical experiments using a set of synthetic test functions and the well-known COCO benchmarking software, we show that the LABCAT algorithm outperforms several state-of-the-art BO and other black-box optimization algorithms.

Keywords: Bayesian optimization, Gaussian processes, black-box optimization, derivative-free optimization, trust region optimization, principal components

1. Introduction

Optimization refers to the fundamental aim of finding the specific set of inputs that maximizes or minimizes a certain objective function, possibly subject to constraints. There is a multitude of optimization strategies to choose from, each with the goal of converging to a local or global solution as quickly and as accurately as possible. Of specific interest for this paper is the problem of so-called “black-box” optimization: an optimization problem where only the output of the objective function can be observed for a given input. These functions may arise when the objective function lacks a closed-form expression or gradient information is unavailable, and are often computationally expensive to evaluate.

One family of optimization methods that addresses the challenge of optimizing expensive black-box functions in a sample-efficient manner is sequential model-based optimization (SMBO) methods. In contrast to traditional optimization techniques, SMBO attempts to approximate the objective function with a *surrogate model* (e.g. Gaussian process [1, 2], random forest [3] or tree-structured Parzen estimator [4]). Each subsequent objective function evaluation is added to this surrogate model, refining the approximation. This next point at which to evaluate the objective function is determined by maximizing an *acquisition function* (e.g. expected improvement (EI) [5] or upper confidence bound (UCB) [6]) that combines exploration of the objective function and exploitation of the best candidate solution. This decision of where to evaluate the objective function according to the acquisition function and refining the surrogate model with this result forms the core loop of SMBO. One prominent member of this family of methods is known as Bayesian

*Corresponding author

Email addresses: emile.visser@gmail.com (E. Visser), cvdaalen@sun.ac.za (C.E. van Daalen), jcschoeman@sun.ac.za (J.C. Schoeman)

optimization (BO) [7] with the Gaussian process (GP) surrogate model¹. BO has been extensively studied [7] and applied to a wide range of problems from hyperparameter optimization for machine learning models [8, 9] to materials and chemical design [10, 11].

BO, however, is no panacea and still has limitations to be aware of. Firstly, it is well-known that BO scales poorly as more observed points are added to the surrogate model (typically in the order $O(n^3)$ [12, Ch. 6] with n observed points). Practically, this limits BO to lower-dimensional problems since a large number of observed points are necessary to model a high-dimensional objective function, leading to computationally expensive calculations. This also leads to BO slowing down significantly with subsequent algorithm iterations as more observations are added to the surrogate model [13]. Sparse approximations, such as the subset of data (SoD) or subset of regressors (SoR) approaches [14], may alleviate this somewhat at the cost of surrogate fidelity.

Secondly, the performance of BO when applied to a specific objective function is dependent on the chosen kernel function, which is a function that defines the family of functions that the GP surrogate model is able to represent. Choosing a single, generic kernel (as is done in the case of a black-box function where there is no prior knowledge of the function) reduces the effectiveness of BO in most situations [15]. This is especially the case where the objective function is either non-stationary, exhibiting different behaviour in different regions; or ill-conditioned, being much more sensitive to certain input variables than others [16].

Finally, while convergence for BO using EI was established by Vasquez and Bect [17], explicit convergence rates depend on strong assumptions on the objective function and exist only for certain kernel functions using fixed hyperparameters, such as in the work of Bull [18] or Srinivas et al. [19]. Bull also showed that for BO using sequentially estimated hyperparameters (a common approach used during BO of black-box functions), BO may not converge at all. Even when these assumptions and criteria for theoretical convergence are met, BO exhibits practical numerical limitations, inhibiting its convergence characteristics. Computational instability in the GP model fitting procedure arises when there is a close proximity between any pair of observed points in the input space, resulting in a near-singular spatial covariance matrix. To address this instability, a common solution is to introduce a small “nugget” parameter δ as diagonal noise [20, 21]. However, this reduces the rate and limit of convergence since an artificial level of noise has been implicitly imposed on the (possibly noiseless) objective function [22].

To summarize, it is clear that standard BO has several shortcomings, namely that it (i) experiences computational slowdown with additional algorithm iterations, (ii) is not well-suited to non-stationary and ill-conditioned functions, and (iii) exhibits poor convergence characteristics.

Related literature. A recent avenue of research to mitigate the noted shortcomings of BO is to introduce a form of local focus, relaxing the global perspective of standard BO. The aim of this approach is to allow BO to leverage global information about the objective function to guide the search towards the optimum and then locally exploit this solution, achieving faster convergence [23, 24]. The prominent algorithms that follow this approach may be loosely categorized into four broad classes.

The first class of algorithms consist of *hybrid* BO algorithms that add some mechanism to BO such that a switch is made to another optimization method with better convergence characteristics at some point during the execution of the algorithm to exploit the best candidate solution. This switch point may be determined according to a metric such as expected gain [13], estimated regret [22] or according to some budget-based heuristic [25]. Unfortunately, determining the optimal switching point is an optimization problem in itself; switching either too early or too late can easily magnify the noted shortcomings of BO while reducing the sample efficiency gained by using BO in the first place.

Another class of algorithms combines BO with *domain partitioning* of the full input space of the objective function into subdivisions. When these subdivisions are ranked, often based on the value of the acquisition function at the centre of the subdivision [26], promising areas can be exploited and further subdivided while others can be ignored in a branch-and-bound fashion. While these methods may have polynomial [27] or even exponential [26] convergence guarantees, they require kernel engineering with prior knowledge of the objective function and scale similarly to standard BO.

¹BO using a GP is also known as efficient global optimization (EGO) [1] and sequential Kriging optimization (SKO) [2].

A different class utilize a combined *local and global kernel*. The mechanism underpinning these methods is that a local kernel is used to model local changes in the objective function while a global kernel models the wider global structure. These kernels may be combined similarly to the piecewise-defined kernel of Wabersich and Toussaint [28] or the weighted linear kernel combination of Martinez-Cantin [15]. While being superior to standard BO when applied to non-stationary problems [15], these algorithms still scale similarly to standard BO and also converge slowly.

The last class of methods uses an adaptive *trust region* to encourage standard BO to exploit the local area surrounding the best candidate solution. This trust region acts as a moving window to constrain the acquisition function and, by extension, limit where the next point of the objective function will be evaluated. This window traverses the objective function and is frequently permitted to expand and contract, guided by a progress-dependent heuristic. Specifically, the window may expand during periods of progress and contract when progress stalls [29, 30, 31]. Alternatively, similar to classical trust-region optimization, the window size may be a function of the quality of the surrogate model’s approximation of the objective function [32, 33, 34]. This trust region modification relaxes the global optimization of standard BO to be more akin to that of robust local optimization, though in practice this approach is sufficient for most problems [30]. To regain a measure of global optimization performance, these methods can be paired with a complementary mechanism such as alternating between a local and a global approximation [32], multistarts with a multi-armed bandit strategy [30] or restarts triggered by a minimum acquisition function threshold [33]. The TuRBO algorithm by Eriksson et al. (TuRBO) [30] also incorporates automatic relevance determination (ARD) [35] through an anisotropic kernel to rescale the side length of the local trust region according to the local smoothness determined by the fitted kernel in a volume preserving transformation. This allows the local trust region to emphasize directions in which the objective function is smoother, a benefit when optimizing separable objective functions. However, the ARD employed by Eriksson et al. [30] is limited to directions defined solely by the coordinate axes. As a result, it may not be able to exploit objective functions that are separable in directions that are not along the coordinate axes. While trust region-based BO methods scale better than standard BO and are more adaptive to non-stationary functions, these methods tend to have poor convergence characteristics and may even terminate prematurely when applied to ill-conditioned functions.

In summary, while current methods may alleviate one or two of the three noted shortcomings of standard BO, none presents a solution that satisfactorily addresses all of them. Among the identified algorithm classes, trust region-based BO exhibits the most promise for addressing all of the noted limitations. Therefore, we propose a novel algorithm which extends the trust region-based approach, offering a solution to alleviate all of the observed shortcomings of standard BO.

Summary of contributions. This paper presents two novel extensions for trust region-based BO. Firstly, we introduce an adaptive trust region- and objective function observation rescaling strategy based on the length-scales of the local GP surrogate with an SE kernel and ARD, instead of a heuristic, to allow for improved convergence characteristics. The second extension is a novel rotation of the trust region to align with the weighted principal components of the observed data. This rotation enables the maximum expressive power of the ARD kernel to model non-stationary and ill-conditioned objective functions. These two extensions are combined in a trust region-based BO framework with an iterative, approximate hyperparameter estimation approach and a subset-of-data (SoD) scheme [14] that greedily discards observations to mitigate computational slowdown, yielding the novel method proposed in this paper, which we denominate as the locally adaptive Bayesian optimization using principal component-aligned trust regions (LABCAT) algorithm.

Using the well-known comparing continuous optimizers (COCO) benchmarking software [36] with the noiseless black-box optimization benchmarking (BBOB) test suite [37], we demonstrate the relative contributions of the novel extensions of the LABCAT algorithm using an ablation study and that the LABCAT algorithm is a leading contender in the domain of expensive black-box function optimization, significantly outperforming standard BO for nearly all tested scenarios and demonstrating superior performance compared to state-of-the-art black-box optimization methods, particularly in the domain of unimodal and highly conditioned objective functions not typically associated with BO.

Structure of the paper. Section 2 gives a brief overview of the requisite theoretical background on Gaussian processes and Bayesian optimization that forms the basis of the proposed LABCAT algorithm. Section 3 presents the proposed algorithm with the length-scale-based and principal component-aligned transformation of the observed points, the iterative estimation of these length-scales, trust region definition, and observation discarding strategy. Section 4 applies the proposed algorithm to several well-known synthetic test functions as well as to the BBOB problem suite [37] from the well-known COCO benchmarking software [36], allowing for a comparison to state-of-the-art black-box optimization algorithms. Relevant proofs and derivations used in Section 3 are included in Appendix A to Appendix D and the full results obtained from the COCO software are given in Appendix E.

2. Preliminaries

In this section, we provide the requisite theoretical frameworks used in the proposed algorithm of Sec. 3. We start this section by reviewing GP regression and the squared exponential (SE) kernel function with automatic relevance determination (ARD) with the maximum a posteriori (MAP) method of estimating the hyperparameters of this kernel function. Finally, we provide an overview of BO with the expected improvement (EI) acquisition function, which is the starting point for the proposed LABCAT algorithm.

2.1. Gaussian process regression

A popular choice of surrogate model for BO is to use Gaussian process (GP), an extension of a multivariate Gaussian distribution to infinite dimensions [12, Ch. 1]. In other words, while multivariate Gaussian distributions describe the behaviour of a finitely long vector of a number of random *variables*, a GP describes the behaviour of a random *function*². This GP model, fitted to n observed d -dimensional input points $X = \{\mathbf{x}_i \in \mathbb{R}^d \mid i \in 1, 2, \dots, n\}$ and observed function values $Y = \{y_i = f(\mathbf{x}_i) \in \mathbb{R} \mid i \in 1, 2, \dots, n\}$ using a mean function $m(\cdot)$ and kernel function $k(\cdot, \cdot)$, can then be used for regression to estimate an unknown function $f(\mathbf{x})$:

$$f(\mathbf{x}) \sim \mathcal{GP}(m(\cdot), k(\cdot, \cdot); X, Y) \quad (1)$$

and infer predictions y_* for input points \mathbf{x}_* using the key assumption of GPs that the posterior distribution for these unobserved points is given by the Gaussian distribution

$$p(y_* \mid \mathbf{x}_*, X, Y) = \mathcal{N}(\mu_{\mathcal{GP}}(\mathbf{x}_*), \sigma_{\mathcal{GP}}^2(\mathbf{x}_*)). \quad (2)$$

To fit a GP to the observed data, a Gram matrix [38] $\mathbf{K} \in \mathbb{R}^{n \times n}$ is constructed using a valid (symmetric and positive semidefinite [12, Ch. 4]) kernel function k , such that each entry satisfies

$$\mathbf{K} = [k(\mathbf{x}_i, \mathbf{x}_j)]_{1 \leq i, j \leq n}. \quad (3)$$

Using this matrix and the column vector $\mathbf{y} = [y_i]_{1 \leq i \leq n}^\top$, the equations for the predicted mean $\mu_{\mathcal{GP}}$ and variance $\sigma_{\mathcal{GP}}^2$ of the GP at a given test point \mathbf{x}_* from (2) are given by [12, Ch. 2]:

$$\mu_{\mathcal{GP}}(\mathbf{x}_*) = m(\mathbf{x}_*) + \mathbf{k}_*^\top \mathbf{K}^{-1}(\mathbf{y} - \mathbf{m}(X)), \quad (4)$$

$$\sigma_{\mathcal{GP}}^2(\mathbf{x}_*) = k(\mathbf{x}_*, \mathbf{x}_*) - \mathbf{k}_*^\top \mathbf{K}^{-1} \mathbf{k}_*, \quad (5)$$

where

$$\mathbf{k}_* = [k(\mathbf{x}_1, \mathbf{x}_*) \quad k(\mathbf{x}_2, \mathbf{x}_*) \quad \dots \quad k(\mathbf{x}_n, \mathbf{x}_*)]^\top.$$

²A naive way to describe a function is to represent it as an infinitely long vector, with each entry specifying the function value $f(x)$. This analogy, while crude, is surprisingly descriptive of the mechanism of a GP.

During the calculation of (4) and (5), determining the inverse matrix \mathbf{K}^{-1} tends to dominate the computation time³ due to matrix inversion being of the order $O(n^3)$ for an $n \times n$ matrix [12, Ch. 6]. This is the principal reason why standard BO typically scales poorly with an increasing number of observations.

2.2. Squared exponential kernel function and hyperparameter estimation

As seen in the previous section, a core component of a GP is a kernel function $k(\cdot, \cdot)$. This function quantifies the notion of similarity between points, as it is a reasonable assumption that input points \mathbf{x} that are similar (read: close together) will typically have similar function values $f(\mathbf{x})$. The kernel function is defined as a map from a pair of inputs $\mathbf{x}_p \in X$ and $\mathbf{x}_q \in X$ to \mathbb{R} where $X \subseteq \mathbb{R}^d$ [39] and must be symmetric positive semidefinite for use in a GP [12, Ch. 4]. This kernel function defines the shape of the functions that the GP will fit to observed points.

Some well-known examples of kernels used in GPs include the Matérn, rational quadratic (RQ) and squared exponential (SE) kernels. While the Matérn kernel is the standard choice for global optimization since it is only twice differentiable versus the infinite differentiability of the SE kernel (a stronger assumption of smoothness that may cause interpolation issues) [9], we have chosen to use the SE kernel. Since we are constructing an iterative local approximation of the objective function, the loss of interpolative precision is acceptable. The SE kernel also has the useful property that the *characteristic length-scale* parameter ℓ of this kernel is strongly correlated with the smoothness of the locally fitted GP model.

The SE kernel can be extended with automatic relevance determination (ARD), which extends the SE kernel with a length-scale parameter for every input dimension $\ell_1 - \ell_d$ [35], allowing the kernel to model differing amounts of variation in each coordinate direction. The definition of this kernel is given as

$$k_{\text{SE}}(\mathbf{x}_p, \mathbf{x}_q) = \sigma_f^2 \cdot \exp\left(-\frac{1}{2}(\mathbf{x}_p - \mathbf{x}_q)^\top \Lambda^{-1}(\mathbf{x}_p - \mathbf{x}_q)\right) + \sigma_n^2 \delta_{pq}, \quad (6)$$

where $\Lambda^{-1} = \text{diag}(\ell_1^2, \ell_2^2, \dots, \ell_d^2)^{-1}$

where σ_f^2 and σ_n^2 are the signal and noise variances respectively. The hyperparameters of this kernel are therefore given by the collection

$$\boldsymbol{\theta} = (\sigma_f, \sigma_n, \ell_1, \ell_2, \dots, \ell_d). \quad (7)$$

A popular method of choosing these hyperparameters is through maximum a posteriori (MAP) estimation, where the hyperparameters $\boldsymbol{\theta}$ are chosen as the maximum of the posterior distribution

$$p(\boldsymbol{\theta} | X, Y) = \frac{p(Y | X, \boldsymbol{\theta})p(\boldsymbol{\theta} | X)}{p(Y | X)}. \quad (8)$$

Since $p(Y | X) = \int_{\boldsymbol{\theta}} p(Y | X, \boldsymbol{\theta})p(\boldsymbol{\theta} | X)d\boldsymbol{\theta}$ is independent of $\boldsymbol{\theta}$. After making the assumption that the prior distribution over the hyperparameters is independent of the observed inputs ($p(\boldsymbol{\theta} | X) = p(\boldsymbol{\theta})$), this is equivalent to maximizing the logarithm of the posterior distribution, or

$$\boldsymbol{\theta}^* = \underset{\boldsymbol{\theta}}{\text{argmax}} (\log p(Y | X, \boldsymbol{\theta}) - \log p(\boldsymbol{\theta})), \quad (9)$$

where, from the logarithmic form of the likelihood function for a multivariate Gaussian, the equation for the marginal log-likelihood $\log p(Y | X, \boldsymbol{\theta})$ is given by

$$\log p(Y | X, \boldsymbol{\theta}) = -\frac{1}{2}\mathbf{y}^\top \mathbf{K}^{-1} \mathbf{y} - \frac{1}{2} \log |\mathbf{K}| - \frac{n}{2} \log 2\pi. \quad (10)$$

This optimization problem in (9) can be solved using existing nonlinear solvers (e.g. BFGS [40]), derivative-free methods (e.g. Nelder-Mead [41]) or stochastic methods (e.g. SGD [42]). It should be noted that evaluating (10) for a new set of hyperparameters also requires recalculating the inverse matrix \mathbf{K}^{-1} , which, as previously mentioned, has a computational complexity of the order $O(n^3)$ with n observed points.

³In practical GP implementations, \mathbf{K}^{-1} is rarely used directly. Since \mathbf{K} is known to be symmetric and positive semidefinite due to the use of a valid kernel function [12, Ch. 4], the Cholesky decomposition of the matrix \mathbf{K} can be used in conjunction with back substitution due to complexity and stability benefits.

2.3. Bayesian optimization

Bayesian optimization attempts to find the argument $\mathbf{x}_{\min} \in \Omega$ that minimizes⁴ a given scalar, bounded, black-box objective function $f(\mathbf{x}) : \mathbb{R}^d \rightarrow \mathbb{R}$, where $\Omega \subset \mathbb{R}^d$ is the set of all possible arguments subject to the specified constraints. In this paper, we assume that f is observable exactly (i.e. with no noise) and parameterize Ω using a Cartesian product with bounding values Ω^{\min} and Ω^{\max} for each dimension. Formally, we can state this optimization task as calculating

$$\mathbf{x}_{\min} = \underset{\mathbf{x}_* \in \Omega}{\operatorname{argmin}} f(\mathbf{x}_*), \quad \text{where } \Omega = \prod_{i=1}^d [\Omega_i^{\min}, \Omega_i^{\max}].$$

In essence, BO iteratively builds a GP surrogate model approximation of the objective function f using points selected according to an acquisition function. The GP is chosen as a surrogate model since it is cheap to evaluate compared to the objective function and the fact that the GP can yield both an estimate of the objective function and the uncertainty of this estimate through the mean and variance of the GP prediction. Using the estimate of the objective function (and uncertainty thereof), an acquisition function is constructed which formalizes the trade-off between exploitation (low GP mean) and exploration (high GP variance) of the objective function.

One popular choice of acquisition function is the expected improvement (EI) function [5], which quantifies the potential of each point to improve on the current minimum observed output value y_{\min} by calculating the expected value of the difference between the estimated value of the surrogate model and the current best function value. The EI function is defined as

$$\alpha_{\text{EI}}(\mathbf{x}_*; \mathcal{GP}) = \sigma_{\mathcal{GP}}(\mathbf{x}_*)[z\Phi(z) + \phi(z)], \quad \text{where } z = \frac{y_{\min} - \mu_{\mathcal{GP}}(\mathbf{x}_*)}{\sigma_{\mathcal{GP}}(\mathbf{x}_*)}$$

and $\phi(z)$ and $\Phi(z)$ is the probability density function and cumulative density function of a univariate standard normal distribution, respectively.

BO may also select an initial set of input points to be observed, known as the design of experiment (DoE), before the main loop of BO starts. This DoE may be constructed using random sampling or more informed methods such as Latin hypercube sampling or Sobol sampling [21] based on the objective function constraints set Ω .

In general, BO does not have a well-defined, general stopping criterion, a property shared with other derivative-free optimization methods. This is in contrast to gradient-based methods, where the norm of the gradient can be used to ensure first-order stationarity of the solution. Consequently, a maximum objective function evaluations or minimum decrease condition is often used as a termination condition for BO.

Algorithm 1 Bayesian Optimization

Input: Objective function f , Acquisition function α , Bounds Ω , Design of experiment DoE

```

1:  $X \leftarrow \text{DoE}(\Omega)$                                  $\triangleright$  Select initial input points using DoE and bounds
2:  $Y \leftarrow \{f(\mathbf{x}) \mid \mathbf{x} \in X\}$                  $\triangleright$  Evaluate initial input points from DoE
3: while not convergence criterion satisfied do
4:    $\mathcal{GP} \leftarrow \mathcal{GP}(m(\cdot), k(\cdot, \cdot); X, Y)$        $\triangleright$  Fit GP with  $X$  and  $Y$ 
5:    $\mathbf{x}_\alpha \leftarrow \operatorname{argmax}_{\mathbf{x}_* \in \Omega} \alpha(\mathbf{x}_*; \mathcal{GP})$    $\triangleright$  Maximize acquisition function
6:    $y_\alpha \leftarrow f(\mathbf{x}_\alpha)$                                  $\triangleright$  Evaluate suggested input point
7:    $X \leftarrow X \cup \{\mathbf{x}_\alpha\}$                              $\triangleright$  Add observed input point to set
8:    $Y \leftarrow Y \cup \{y_\alpha\}$                                  $\triangleright$  Add observed output point to set
9: end while
10: return  $\mathbf{x}_{\min}, y_{\min}$                                  $\triangleright$  Return minimum candidate

```

⁴An arbitrary choice, since any minimization problem can be converted to a maximization problem with a simple sign change in the objective function.

The BO algorithm is summarized in Alg. 1, where the inner loop of selecting an input point that maximizes the acquisition function α , evaluating the objective function f at this point, adding the result to the isomorphic sets of observed points X and Y , and refitting the model with the augmented observations is given in lines 3 – 9. This algorithm forms the foundation for the proposed algorithm in the next section. The proposed algorithm’s primary change is an adaptive rescaling- and rotation strategy based on the surrogate GP model for X and Y , as well as an iteratively updated trust region to bound the acquisition function and a greedy strategy for discarding observations from X and Y that fall outside of this trust region.

3. Proposed LABCAT algorithm

The novel method proposed in this paper, which we denote as the locally adaptive Bayesian optimization using principal component-aligned trust regions (LABCAT) algorithm, follows the example of other trust region BO algorithms by incorporating a local trust region surrounding the current minimum candidate solution to bound the acquisition function maximization during the determination of subsequent input points [29, 30, 31, 32, 33, 34]. What distinguishes LABCAT is that, instead of according to a progress-based or sufficient decrease heuristic, the size of this local trust region is selected to be directly proportional to the length-scales of the GP fitted to the observed data. This trust region is also rotated to align with the weighted principal components of the observed data, allowing the size of the trust region to change along arbitrary directions, not just along the coordinate axes. Additionally, the trust region is used to greedily discard observed points outside of the trust region, in contrast to the noted methods that either retain all points or employ a significant subset of the evaluation history. A flowchart depicting the LABCAT algorithm is shown in Fig. 1, with the full description of the algorithm given at the end of this section.

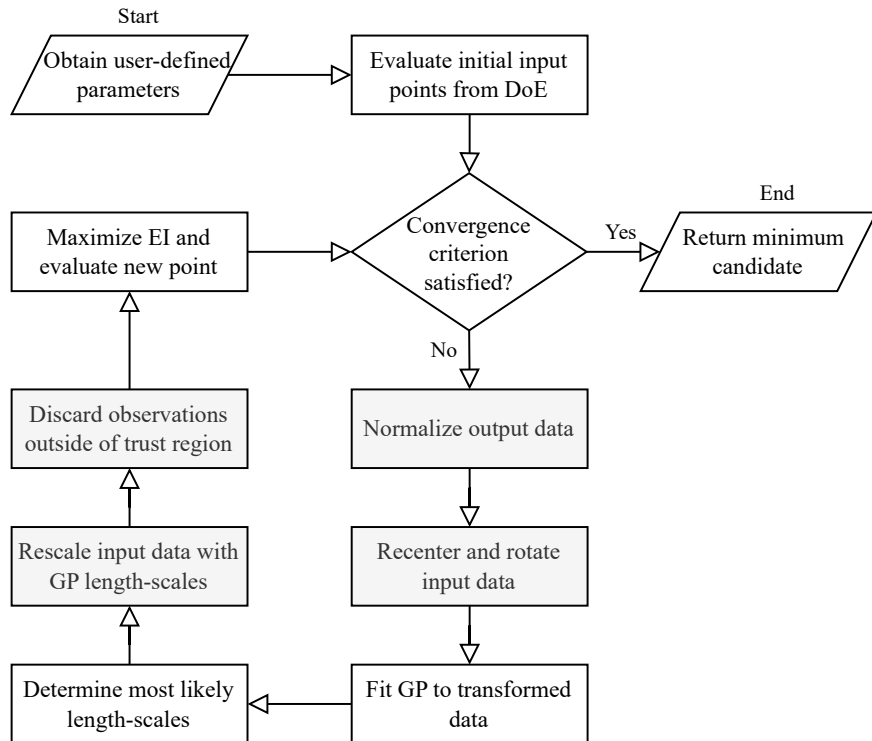


Figure 1: A flowchart of the locally adaptive Bayesian optimization using principal component-aligned trust regions (LABCAT) framework. The primary additions to the standard BO algorithm is given by the shaded components.

Inspecting Fig. 1, the algorithm enters a modified version of the standard BO loop after evaluating the initial set of input points. These modifications consist of transforming the observed data, bounding the

acquisition function with a trust region, and discarding observations that fall outside of this trust region. At the start of the modified BO loop, the current set of observed inputs are recentred on the current minimum candidate and rotated in such a way that the principal components of the observed input points (weighted by the corresponding normalized observed output values) are aligned with the coordinate axes. Using this recentred, rotated and normalized observed input and output data, a GP with an SE kernel with ARD is fitted. The MAP estimate for the length-scales of this kernel is then determined and used to rescale the observed input data, updating the size of the current trust region. To prevent the unbounded growth in complexity of the GP model that leads to the noted computational slowdown of standard BO (Sec. 2.1), we make use of an approximate model fitted to the local subset of observations that lie in the current trust region, discarding any observations outside of the trust region. Finally, the EI acquisition function is maximized, bounded by the trust region, to determine the next input point to be evaluated.

The rest of this section describes each of the salient components of the LABCAT algorithm: the transformations applied to the observed data, the calculation of kernel hyperparameters for the fitted GP, the definition of the trust region used for the bounding of the EI maximization and the mechanism for discarding observations. This section concludes with the chosen convergence criteria, choice of initial observed points, and an overview of the LABCAT algorithm.

3.1. Transformed representation

During the course of a trust region-based BO algorithm, the size of the trust region necessarily shrinks as the algorithm converges to a solution. This shrinking trust region may lead to observations being clustered together or ill-conditioned, leading to the noted near singularity of the spatial covariance matrix \mathbf{K} . To ameliorate this, we transform the observations to a transformed space in which we perform minimization actions that work well for a much smaller range of objective function values compared to the original space. In this transformed space, the observations remain well-conditioned and -distributed, even if the corresponding points in the objective function space are not. Ideally, this transformed space is also rotated to allow for the maximum expressive potential of the chosen kernel function (SE with ARD from (6)) when fitting a GP in this transformed space, for example, aligning the length-scales of the ARD kernel with possible directions of separability in the observed data.

To do this, we construct an invertible mapping between the observed data X, Y and a transformed representation X', Y' of the same dimensionality, that is, $X \subset \mathbb{R}^d \leftrightarrow X' \subset \mathbb{R}^d$ and $Y \subset \mathbb{R} \leftrightarrow Y' \subset \mathbb{R}$, according to a set of invariant properties (i)–(iv) that are preserved at each algorithm iteration. As can be seen in Fig. 1 and in the example of Fig. 2, these invariant properties are preserved through the recentring and rotation of the observed input data, the normalization of the output data, and the rescaling of the observed input data according to the local length-scales of a GP.

For notational convenience, we indicate the image of a variable under this transformation by using the primed counterpart of the variable and vice versa for the preimage, for example, the variable x and the image of this variable under the transformation x' . Furthermore, in this section a set X' can be collected into and decomposed from a matrix $\mathbf{X}' \in \mathbb{R}^{d \times n}$, where the i^{th} column of \mathbf{X}' corresponds to \mathbf{x}'_i in X' .

Transformation definition. For the transformation of the input points from X to X' , we construct the following affine transformation between the elements of these sets

$$\mathbf{x}_i = \mathbf{R}\mathbf{S}\mathbf{x}'_i + \mathbf{b}_x \quad \forall i \in \{1, 2, \dots, n\}, \quad (11)$$

using a scaling matrix \mathbf{S} , rotation matrix \mathbf{R} and offset vector \mathbf{b}_x . This transformation naturally extends to a relation expressed using the matrices \mathbf{X} and \mathbf{X}'

$$\mathbf{X} = \mathbf{R}\mathbf{S}\mathbf{X}' + \mathbf{b}_x \mathbf{1}_n^\top, \quad (12)$$

with the transformation parameters \mathbf{R} , \mathbf{S} and \mathbf{b}_x calculated according to three invariant properties. These invariant properties are defined as the following:

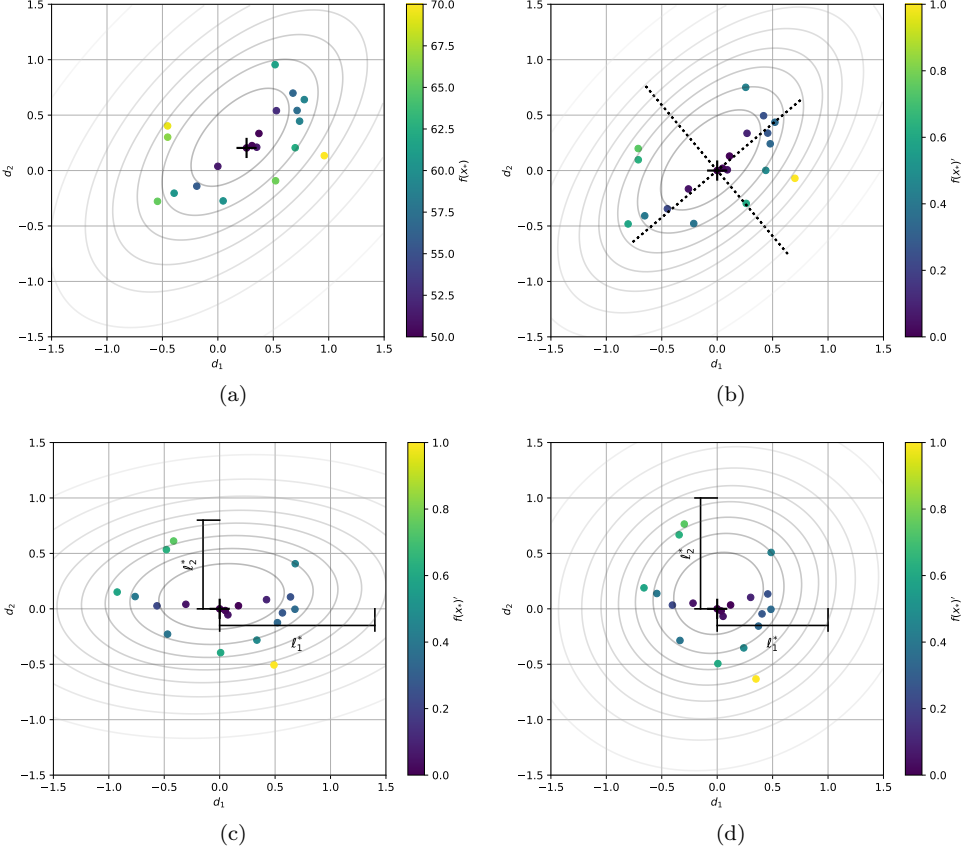


Figure 2: A visualization of enforcing the invariant properties (described by (i)–(iv)) on (a) a number of observations from an arbitrary function, where the observed output values are represented using a colour map. (b) The data is centred on the minimum candidate (marked with a +) and the output values are normalized. This transformed data is also used to calculate the weighted principal components (shown with the dashed line). (c) The observed input data is rotated so that the weighted principal components align with the coordinate axes, and the most likely length scales (ℓ_1^* , ℓ_2^*) for a GP fitted to the data are shown. (d) Finally, the input data is rescaled such that these length-scales equal unity, with all invariant properties now preserved.

(i) The transformed input point \mathbf{x}'_{\min} , which is the corresponding transformed point of the current minimum candidate $\mathbf{x}_{\min} = \{\mathbf{x}_i \in X \mid y_i \leq y_j, \forall y_j \in Y\}$, is at the origin

$$\mathbf{x}'_{\min} = [0 \quad \dots \quad 0]^{\top}. \quad (13)$$

(ii) The weighted principal components, described by the orthogonal rotation matrix \mathbf{U} of the observed input data X , centred on the current minimum candidate and with more weight given to values of X with a lower corresponding value in Y , are transformed to be aligned with the coordinate axes of X' (up to reflection)

$$\mathbf{U} \mapsto \mathbf{U}' = \text{diag}(\pm 1, \dots, \pm 1). \quad (14)$$

(iii) X' is scaled such that the most likely length-scales ℓ^* for a GP that has been fitted with X' and Y' are unity, or

$$\ell^* = (1, 1, \dots, 1). \quad (15)$$

Similarly to (11), we construct a relation between the observed outputs Y and a set of transformed outputs Y' as

$$y_i = a \cdot y'_i + b_y \quad \forall i \in \{1, 2, \dots, n\} \quad (16)$$

according to an additional invariant property which states:

- (iv) The current minimum observed output value y_{\min} and the the maximum observed value y_{\max} are min-max normalized

$$y'_{\min} = 0 \quad \text{and} \quad y'_{\max} = 1. \quad (17)$$

Invariant property preservation. To preserve the invariant properties of the transformed input data defined in (i)–(iv) requires four steps. Firstly, the invariant property of the output data from (iv) is preserved by transforming Y' using the values of y_{\min} and y_{\max} with min-max normalization [43]

$$Y' = \left\{ \frac{y_i - y_{\min}}{y_{\max} - y_{\min}} \mid y_i \in Y \right\} \quad (18)$$

and by setting the output offset and scaling coefficients to

$$a = y_{\max} - y_{\min} \quad \text{and} \quad b_y = y_{\min}. \quad (19)$$

For the next step, we enforce invariant property (i) through recentring X with the current minimum candidate \mathbf{x}_{\min} , subtracting this value from every element of X . This is achieved using the transform

$$\mathbf{X}_{\text{cen}} = \mathbf{X} - \mathbf{x}_{\min} \mathbf{1}_n^\top \quad (20)$$

and by setting the offset vector \mathbf{b}_x to

$$\mathbf{b}_x = \mathbf{x}_{\min}. \quad (21)$$

Next, to enforce invariant property (ii), we use the the sample-wise weighted, centred input data $\mathbf{X}_{\text{cen}} \mathbf{W}$ to calculate the weighted principal components \mathbf{U} . We calculate these weighted principal components \mathbf{U} using the singular value decomposition (SVD) [44] with the following form

$$\mathbf{X}_{\text{cen}} \mathbf{W} = \mathbf{U} \Sigma \mathbf{V}^\top, \quad (22)$$

with this weight matrix constructed with sample-wise weights chosen, leveraging invariant property (iv) of the output data Y' , to be biased toward lower output values. These weights are be determined by subtracting each element of Y' from 1 and aggregating into a diagonal matrix

$$\mathbf{W} = \text{diag}(1 - y'_1, 1 - y'_2, \dots, 1 - y'_n). \quad (23)$$

Note that, since \mathbf{X}_{cen} and \mathbf{W} are real matrices, the rotation matrix \mathbf{U} obtained through the SVD is orthogonal and, therefore, $\mathbf{U}^{-1} = \mathbf{U}^\top$. Using this fact, multiplying the inverse rotation matrix with \mathbf{X}_{cen} aligns the weighted principal components of the product with the coordinate axes, since $\mathbf{U}^\top \mathbf{U} \Sigma \mathbf{V}^\top = \mathbf{I} \Sigma \mathbf{V}^\top$, given by

$$\mathbf{X}_{\text{rot}} = \mathbf{U}^\top \mathbf{X}_{\text{cen}} \quad (24)$$

and the rotation matrix \mathbf{R} in (11) is set to

$$\mathbf{R} = \mathbf{U}. \quad (25)$$

Ideally, this alignment of the coordinate axes of X' with the weighted principal axes of X assists in uncovering local separability that can be well-modelled by the ARD kernel, for example, a local valley in the objective function.

Finally, we fit a GP to X_{rot} and Y' using an SE kernel with ARD as in (6) and determine the most likely length-scales ℓ^* using (9). Using ℓ^* , invariant property (iii) is preserved by scaling the rotated transformed input data X_{rot} according to

$$X' = \mathbf{L}^{-1} \mathbf{X}_{\text{rot}} \quad (26)$$

where the most likely length-scales are collected into a scaling matrix

$$\mathbf{L}^{-1} = \text{diag}(\ell_1^*, \ell_2^*, \dots, \ell_n^*)^{-1}. \quad (27)$$

and the scaling matrix \mathbf{S} in (11) is set to

$$\mathbf{S} = \mathbf{L}, \quad (28)$$

with no need to recalculate the kernel matrix \mathbf{K} for the GP fitted to X_{rot} , Y' and ℓ^* , as both the observed inputs and length-scales have been scaled by the same factor. Inspecting (6) and factorizing the individual length-scales, this rescaled GP is now equivalent to a GP fitted to X' and Y' with unit length scales.

Iterative transformation calculation. During the execution of the LABCAT algorithm, it is not necessary to perform a full recalculations of X' and Y' from X and Y at each algorithm iteration. Instead, we leverage the transformed representations obtained from the preceding algorithm iteration, denoted as X'_{old} and Y'_{old} . These transformed representations may incorporate added or removed observations such that the invariant properties no longer hold. Moreover, we retain the previous transformation parameters, also indicated by the subscript ‘‘old.’’ To efficiently restore the invariant properties for these values from the preceding algorithm iteration, we calculate X' and Y' with the associated transformation parameters in terms of the values from the previous algorithm iteration. Note that the initial values and transformation parameters for the LABCAT algorithm uses a modified version of this transform based on the bounds of the objective function Ω and is given in Sec. 3.4.

Firstly, the transformed outputs of the previous iteration Y'_{old} are renormalized using the minimum- and maximum values of this set, $y'_{\min, \text{old}}$ and $y'_{\max, \text{old}}$, as

$$Y' = T_{\min\text{-}\max}(Y'_{\text{old}}) = \left\{ \frac{y'_{i, \text{old}} - y'_{\min, \text{old}}}{y'_{\max, \text{old}} - y'_{\min, \text{old}}} \mid y_{i, \text{old}} \in Y_{\text{old}} \right\} \quad (29)$$

and the transformation parameters in the output transformation from (16) are calculated as

$$\begin{aligned} b_y &= b_{y, \text{old}} + y'_{\min, \text{old}} \cdot k_{\text{old}}, \\ a &= a_{\text{old}} \cdot (y'_{\max, \text{old}} - y'_{\min, \text{old}}). \end{aligned} \quad (30)$$

Invariant property (i) is preserved by recentering \mathbf{X}'_{old} on the (possibly new) minimum candidate $\mathbf{x}'_{\min, \text{old}}$ with

$$T_{\text{cen}}(X'_{\text{old}}) = \mathbf{X}'_{\text{cen}} = \mathbf{X}'_{\text{old}} - \mathbf{x}'_{\min, \text{old}} \mathbf{1}_n^\top, \quad (31)$$

with the offset vector \mathbf{b}_x updated using the value of the previous iteration and the (possibly new) minimum candidate

$$\mathbf{b}_x = \mathbf{b}_{x, \text{old}} + \mathbf{R}_{\text{old}} \mathbf{S}_{\text{old}} \mathbf{x}'_{\min, \text{old}}. \quad (32)$$

Next, to restore invariant property (ii) we inspect the transform defined in (12). We can see that multiplying the transformed input data \mathbf{X}' by the scaling matrix \mathbf{S} yields a representation of the data in an intermediate, affine space of the original input space of X . This intermediate space is equivalent to

a recentred and rotated affine space of the original space of \mathbf{X} . After calculating the weighted principal components \mathbf{U}_a in this intermediate space

$$\mathbf{S}\mathbf{X}'_{\text{cen}}\mathbf{W} = \mathbf{U}_a\boldsymbol{\Sigma}_a\mathbf{V}_a^\top \quad (33)$$

we can use this rotation matrix \mathbf{U} , after a change of basis using \mathbf{S} from the intermediate space, to rotate \mathbf{X}'_{cen} using the transform

$$\mathbf{X}'_{\text{rot}} = T_{\text{rot}}(\mathbf{X}'_{\text{cen}}) = \mathbf{S}_{\text{old}}^{-1}\mathbf{U}_a^\top\mathbf{S}_{\text{old}}\mathbf{X}'_{\text{cen}} \quad (34)$$

and calculate the transformation parameter \mathbf{R} in terms of the value from the previous iteration

$$\mathbf{R} = \mathbf{R}_{\text{old}}\mathbf{U}_a, \quad (35)$$

essentially updating the rotational component of the transformation defined in (11) without requiring the full transformation of \mathbf{X}' back to \mathbf{X} .

Finally, similarly to (26), we use the most likely length-scales for a GP fitted to \mathbf{X}'_{rot} and \mathbf{Y}' to rescale \mathbf{X}'_{rot} according to

$$\mathbf{X}' = T_{\text{resc}}(\mathbf{X}'_{\text{rot}}) = \mathbf{L}^{-1}\mathbf{X}'_{\text{rot}} \quad (36)$$

and recalculate the transformation parameter \mathbf{S} in terms of the value from the previous iteration

$$\mathbf{S} = \mathbf{L}\mathbf{S}_{\text{old}}, \quad (37)$$

also essentially updating the scaling component of the transformation defined in (11) without requiring the full transformation of \mathbf{X}' back to \mathbf{X} .

Proofs for the validity of these updates are given in Appendix A to Appendix C. This cyclical process of recentering, rescaling and rotation ensures that the transformed \mathbf{X}' and \mathbf{Y}' remain well-conditioned, even if the corresponding observations in the objective space \mathbf{X} and \mathbf{Y} become ill-conditioned or clustered closely together. The rotation performed in (34) also ensures that the ARD kernel, as defined in (6), can effectively leverage local separability within the objective function, aligning the axes of each ARD length-scale with the axes of local separability.

3.2. GP hyperparameter estimation

In the previous section describing the transformation from the original observations \mathbf{X} and \mathbf{Y} to transformed representations \mathbf{X}' and \mathbf{Y}' , one of the steps is to preserve the length-scale invariant property described in (iii) by calculating the most likely length-scales $\boldsymbol{\ell}^*$ for a GP fitted to the recentred, rotated \mathbf{X}'_{rot} from (34) and normalized output values \mathbf{Y}' from (29). Instead of the conventional approach of a full re-estimation of the kernel hyperparameters $\boldsymbol{\theta}^*$ using the maximization of the MAP estimate in (9) at each algorithm iteration or once every N iterations, we adopt an approximative scheme. In this approach, the approximate hyperparameters for the local GP model are calculated at each algorithm iteration using a small number of optimization steps, tending towards the exact hyperparameters with subsequent *algorithm iterations*, not with additional *optimization steps* per algorithm iteration. Using a fixed number of optimization steps per algorithm iteration, instead of executing as many optimization steps as necessary for convergence of the hyperparameters, results in computational advantages by reducing the number of operations with a complexity of $O(n^3)$ (recalculating the \mathbf{K}^{-1} matrix from Sec. 2.2) performed during each algorithm iteration.

We set the mean function $m(\cdot)$ of the GP to the mean of the transformed output data \mathbf{Y}' and choose to set the noise variance to $\sigma_n = 10^{-6}$ in our chosen kernel function from (6) to function as a small ‘‘nugget’’ term for increased numerical stability [20]. This prevents the kernel matrix \mathbf{K} in (3) from becoming singular if the observed points become very correlated by slightly inflating the uncertainty of the observed output values, in effect, adding a small offset to the diagonal entries of the kernel matrix. While the standard approach is to optimize σ_f directly, we decide to set this parameter to a fixed value of the standard deviation of \mathbf{Y}' at

each algorithm iteration. Due to the continuous rescaling of the outputs described in (29), the algorithm is not very sensitive to this choice.

With these design choices, the hyperparameters to be optimised are reduced to the length-scales of the kernel $\boldsymbol{\ell}$ for the GP fitted in the transformed space of X'_{rot} and Y' . The derivatives of the log-likelihood surface from (10) with respect to the length-scales $\boldsymbol{\ell}$ [45], with the transformation such that the derivatives are with respect to the length-scales in logarithmic space to ensure that parameters are strictly positive, are given by the Jacobian defined as

$$\nabla \log p(Y' | X'_{\text{rot}}, \boldsymbol{\theta}) = \mathbf{J} := \left[\frac{\partial \log p(Y' | X'_{\text{rot}}, \boldsymbol{\theta})}{\partial \ln \ell_i} \right]_{1 \leq i \leq d} \in \mathbb{R}^{d \times 1} \quad (38)$$

and Hessian

$$\nabla^2 \log p(Y' | X'_{\text{rot}}, \boldsymbol{\theta}) = \mathbf{H} := \left[\frac{\partial^2 \log p(Y' | X'_{\text{rot}}, \boldsymbol{\theta})}{\partial \ln \ell_i \partial \ln \ell_j} \right]_{1 \leq i, j \leq d} \in \mathbb{R}^{d \times d} \quad (39)$$

where $\frac{\partial \log p(Y' | X'_{\text{rot}}, \boldsymbol{\theta})}{\partial \ln \ell_i}$ and $\frac{\partial^2 \log p(Y' | X'_{\text{rot}}, \boldsymbol{\theta})}{\partial \ln \ell_i \partial \ln \ell_j}$ for the SE kernel with ARD from (6) are given in Appendix D.

One would logically expect, with respect to BO with a local trust region, that the most likely length-scales for a GP fitted to a trust region typically exhibit mostly gradual changes as the trust region shifts. Thus, if the most likely length-scales are calculated for a GP fitted to a locally constrained window and a new potential minimum is determined, causing a slight shift in the window's location, the hyperparameters for the new window are expected to be similar to the previous values. To incorporate this assumption, similarly to the technique in [46], we place a Gaussian prior centred on 1 (0 in log-space) over the length-scales. This augmentation effectively restrains the GP from making abrupt changes in hyperparameters, ensuring the stability of the algorithm. We suggest setting the standard deviation of this prior σ_{prior} to a value of approximately 0.1, such that, by the three-sigma rule of thumb, the side lengths of the local trust region is unlikely to change by more than 30% per algorithm iteration. Consequently, the log-likelihood formula from (10) is augmented with this new term (ignoring normalization constants) and is given by

$$\log p(Y' | X'_{\text{rot}}, \boldsymbol{\theta}, \sigma_{\text{prior}}) = \log p(Y' | X'_{\text{rot}}, \boldsymbol{\theta}) - \sum_{i=1}^d \frac{\ln \ell_i^2}{2\sigma_{\text{prior}}^2}, \quad (40)$$

with the Jacobian defined in (38) augmented as

$$\nabla \log p(Y' | X'_{\text{rot}}, \boldsymbol{\theta}, \sigma_{\text{prior}}) = \mathbf{J} - \frac{1}{\sigma_{\text{prior}}^2} \ln \boldsymbol{\ell} \quad (41)$$

and the Hessian defined in (39) augmented as

$$\nabla^2 \log p(Y' | X'_{\text{rot}}, \boldsymbol{\theta}, \sigma_{\text{prior}}) = \mathbf{H} - \frac{1}{\sigma_{\text{prior}}^2} \mathbf{I}. \quad (42)$$

Upon the calculation of these Jacobian and Hessian matrices, if \mathbf{H} is negative definite (all of the eigenvalues of \mathbf{H} are negative) it can be concluded that the current hyperparameters are in a convex-down region of the log-likelihood space. Consequently, a second-order Newton step can be effectively employed. Conversely, if \mathbf{H} is not negative definite, a gradient ascent step is used. Both of these steps are combined with a backtracking line search [47] to determine the optimal step length.

Considering the rescaling of the input data performed in (36), the calculation of the most likely length-scales during each algorithm iteration can be interpreted as an indication to expand or contract each of the dimensions of the transformed input data X' . If X' is never recentred, additional observations allow the GP to construct a more accurate model of the objective function and the length-scales of this better GP model will tend to unity with subsequent observed points.

3.3. Trust region definition and observation discarding

A key mechanism of trust region-based BO is limiting the region of the acquisition function around the best candidate solution in which the next point is observed by means of a trust region. In the LABCAT algorithm, after the set of observations X is transformed to X' according to the invariant properties (i) and (iii), that is, transformed such that the most likely length-scales of the kernel are unity ($\ell^* = \{\ell_i = 1 \mid i \in 1, 2, \dots, n\}$) and that the observed inputs are centred on the current minimum candidate ($\mathbf{x}'_{\min} = [0 \ \dots \ 0]^\top \in X'$), a trust region Ω_{TR} is constructed in the space of X' as a closed, compact d -cube with a side length of 2β . Using the Cartesian product, this trust region is defined as

$$\Omega_{\text{TR}} = [-\beta, \beta]^d, \quad (43)$$

where β is a tunable parameter that captures the trade-off between the exploration of the region surrounding and the exploitation of the current minimum value. Small values for β strongly encourage local exploitation, but may lead to small step sizes. In the case where β tends to infinity, the algorithm will search for the next point in an unconstrained manner and revert back to the global optimization of standard Bayesian optimization. For this parameter, we recommend values in the interval $0.1 \leq \beta \leq 1$ according to the rough heuristic $\beta \approx \frac{1}{d}$. In our experience, these range of values provide a good trade-off, preventing the trust region from growing infinitely and encouraging convergence to a local optimum.

It is important to note that there is slight a difference between the trust region used by LABCAT and those used by other, more classical methods. Instead of the size of the trust region being directly modified inside the fixed space of the original observations X , in the LABCAT algorithm the size of the trust region is specified by (43) in the transformed space of observations X' and it is this space that is scaled. In effect, this induces a trust region in the original objective function space of X without requiring the transformation of X' back to X .

The trust region-bounded acquisition function, chosen as EI in this paper (Sec. 2.3)⁵, is maximized using L-BFGS-B [40] with $10d$ random restarts distributed across Ω_{TR} according to a space-filling quasi-random Sobol sequence [50, 21] and the box constraints of L-BFGS-B are set to Ω_{TR} . The results obtained from this maximization are also validated against the original constraints of the objective function Ω using rejection sampling after transforming the points back into the objective function space using the inverse of the transform defined in (11), in effect, maximizing over the intersection of Ω and Ω_{TR} , or

$$\mathbf{x}'_{\text{ei}} = \underset{\substack{\mathbf{x}'_* \in \Omega_{\text{TR}} \\ \mathbf{x}_* \in \Omega}}{\text{argmax}} \alpha_{\text{ei}}(\mathbf{x}'_*; \mathcal{GP}). \quad (44)$$

Apart from limiting the region in which the next observation should be chosen, the trust region Ω_{TR} is also used to determine which observed points from X' and Y' should be preserved at each algorithm iteration. We assume that observations outside this trust region no longer contribute significant information, therefore, we discard these observations. This keeps the number of observations in the model and, by extension, the computation time per algorithm iteration relatively constant across the runtime of the algorithm, alleviating the noted computational slowdown of standard BO (Sec. 2.1)⁶.

A minimum number of observations are preserved at each algorithm iteration, even if some may fall outside of the trust region, as there may be cases where discarding enough observations cause the observation set to become rank-deficient, occurrences that may lead the fitted GP to make dramatic changes to the length-scales. We denote this parameter m such that the minimum number of preserved observations is m multiples of the objective function dimensionality d . The operation applied to X' , removing the observations in the set X'_{rem} if the size of X' is larger than md , is defined as

⁵Note that many alternative acquisition functions have been proposed [6, 48, 49] and while we have chosen EI for simplicity, other acquisition functions could potentially be substituted for EI in our proposed algorithm.

⁶It is also not necessary to recalculate the kernel matrix, and the inverse/Cholesky decomposition thereof, for the reduced set of observations. The corresponding rows and columns of the observations in X'_{rem} can be removed from \mathbf{K} while efficient updates can be applied to \mathbf{K}^{-1} in terms of the Schur complement [51] or rank-1 downdates of the Cholesky decomposition of \mathbf{K} , both of the order of $O(n^2)$.

$$T_{\text{discard}}(X', Y') = \begin{cases} (X', Y') & |X'| \leq md \\ (X' \setminus X'_{\text{rem}}, Y' \setminus \{y'_i \mid \mathbf{x}'_i \in X'_{\text{rem}}\}) & |X'| > md \end{cases} \quad (45)$$

with the input observations to be discarded chosen, prioritizing older observations, to be those that fall outside the current trust region ($\forall \mathbf{x}' \in X'_{\text{rem}}, \mathbf{x}' \notin \Omega_{\text{TR}}$) until the size of X' reaches the md threshold. Note that that in this operation, the current minimum candidate solution \mathbf{x}'_{\min} is guaranteed to be preserved due to invariant property (i), which guarantees that this candidate is moved to the origin, an element of Ω_{TR} by definition. The corresponding elements from Y' are also removed to ensure that X' and Y' retain a one-to-one correspondence.

This cache size factor m is a user-specified parameter and a poor choice thereof may lead to suboptimal performance characteristics. For instance, if m is set too low, the model GP fitted to X' and Y' may have too few observations to model the objective function. Conversely, if m is set too high, the algorithm may become sluggish as it struggles to discard old, non-informative observations quickly enough to keep up with the moving trust region. Bearing these remarks in mind, we recommend a value in the interval $5 \leq m \leq 10$.

3.4. Algorithm initialization and termination

During the initialization of the LABCAT algorithm, similarly to standard BO, a set of initial points are chosen to be evaluated before the main loop begins, known as the design of experiment (DoE). Using the provided input domain Ω , the DoE for the initial GP surrogate model X is distributed according to a Latin hypercube design [52] with $2d + 1$ points to ensure full rank. Latin hypercube sampling (LHS) was chosen for the initial points to avoid clustering of the initial points, which might occur with random sampling, and to capture as much projected variance along the objective function's coordinate axes as possible.

After observing these initial points X and Y from the objective function, the upper- and lower bounds placed on the objective function used to define Ω ($\{(\Omega_i^{\min}, \Omega_i^{\max}) \mid i \in 1, 2, \dots, d\}$) are used to initialize the respective transformed representations X' and Y' . To do this, we adapt the mechanisms used to enforce the invariant properties (i), (iii) and (iv), with the modification that X' is centred on the midpoint of the bounds, no rotation is performed and the bounds are rescaled to lie on the hypercube $[-1, 1]^d$ (in other words, unit length from the origin in each dimension). This modification ensures that initial observations from the DoE are well-conditioned, but also that the invariant properties (i)–(iii) temporarily no longer hold until the first algorithm iteration completes. The modified transformation to initialize X' and Y' is given by

$$(X', Y') = T_{\Omega}(X, Y, \Omega) = \left(\mathbf{D}^{-1}(\mathbf{X} - \mathbf{c}\mathbf{1}^{\top}), \left\{ \frac{y_i - y_{\min}}{y_{\max} - y_{\min}} \mid y_i \in Y \right\} \right) \quad (46)$$

where the scaling matrix \mathbf{D} and offset vector \mathbf{c} are constructed using Ω according to

$$\mathbf{D}^{-1} = \text{diag} \left(\frac{|\Omega_1^{\max} - \Omega_1^{\min}|}{2}, \frac{|\Omega_2^{\max} - \Omega_2^{\min}|}{2}, \dots, \frac{|\Omega_d^{\max} - \Omega_d^{\min}|}{2} \right)^{-1},$$

and $\mathbf{c} = \left[\frac{\Omega_1^{\max} + \Omega_1^{\min}}{2} \quad \frac{\Omega_2^{\max} + \Omega_2^{\min}}{2} \quad \dots \quad \frac{\Omega_d^{\max} + \Omega_d^{\min}}{2} \right]^{\top}$. (47)

The input transformation parameters \mathbf{S} , \mathbf{R} and \mathbf{b}_x are initialized as

$$\mathbf{S} = \mathbf{D}, \mathbf{R} = \mathbf{I} \quad \text{and} \quad \mathbf{b}_x = \mathbf{c} \quad (48)$$

with the output transformation parameters initialized as

$$a = y_{\max} - y_{\min} \quad \text{and} \quad b_y = y_{\min}. \quad (49)$$

As with standard BO, the LABCAT algorithm has no specific convergence criterion (Sec. 2.3) and may terminate as specified by the user if either (i) the current candidate minimum output y_{\min} is less than some target value, (ii) if the range of output values in Y (captured by the variable a) falls below some tolerance or (iii) the maximum objective function evaluation budget is reached.

3.5. LABCAT algorithm overview

Synthesizing the detailed descriptions from Sec. 3.1–3.4 of the salient components of the LABCAT algorithm, as seen in Fig. 1, the LABCAT algorithm is given in Alg. 2.

Algorithm 2 LABCAT

Input: Objective function f , Bounds Ω , Trust region size factor β , Observation cache size factor m , Length-scale prior standard deviation σ_{prior}

```

1:  $X \leftarrow \text{LATINHYPERCUBESAMPLING}(\Omega)$                                 ▷ Select initial DoE with Latin hypercube over bounds.
2:  $Y \leftarrow \{f(\mathbf{x}) \mid \mathbf{x} \in X\}$                                          ▷ Evaluate objective function at initial input points.
3:  $(X', Y') \leftarrow T_{\Omega}(X, Y, \Omega)$                                          ▷ Initialize transformed representation of observed data (see (46)).
4:  $\Omega_{\text{TR}} \leftarrow [-\beta, \beta]^d$                                          ▷ Construct trust region  $d$ -cube (see Sec. 3.3).
5: while not converged do
6:    $Y' \leftarrow T_{\text{min-max}}(Y')$                                          ▷ Normalize observed output values (see (29)).
7:    $X'_{\text{rot}} \leftarrow T_{\text{rot}}(T_{\text{cen}}(X'))$                                          ▷ Centre obs. inputs using current min. candidate and
                                                rotate with weighted principal components (see (31, 34))
8:    $\mathcal{GP} \leftarrow \mathcal{GP}(m(\cdot), k_{\text{SE}}(\cdot, \cdot); X'_{\text{rot}}, Y')$                                          ▷ Fit GP with an SE kernel with
                                                ARD to  $X'_{\text{rot}}$  and  $Y'$ , (see Sec. 2.1).
9:    $\ell^* \leftarrow \text{argmax}_{\ell}(\log p(Y' \mid X'_{\text{rot}}, \ell) - \log p(\ell \mid \sigma_{\text{prior}}))$  ▷ Find most likely length-scales (see Sec. 3.2).
10:   $X' \leftarrow T_{\text{resc}}(X'_{\text{rot}})$                                          ▷ Rescale obs. inputs with most likely length-scales (see (36)).
11:   $(X', Y') \leftarrow T_{\text{discard}}(X', Y')$                                          ▷ Discard observations if over  $md$  threshold (see (45)).
12:   $\mathbf{x}'_{\text{ei}} \leftarrow \text{argmax}_{\substack{\mathbf{x}'_* \in \Omega_{\text{TR}} \\ \mathbf{x}_* \in \Omega}} \alpha_{\text{EI}}(\mathbf{x}'_*; \mathcal{GP})$                                          ▷ Maximize EI acquisition function over
                                                trust region and bounds (see (2.3)).
13:   $y_{\text{ei}} \leftarrow f(\mathbf{x}_{\text{ei}})$                                          ▷ Evaluate suggested input point from objective
                                                function, transformed according to (11).
14:   $X' \leftarrow X' \cup \{\mathbf{x}'_{\text{ei}}\}$                                          ▷ Append suggested input point.
15:   $Y' \leftarrow Y' \cup \{y'_{\text{ei}}\}$                                          ▷ Append evaluated output value, transformed according to (11).
16: end while
17: return  $\mathbf{x}_{\min}$ ,  $y_{\min}$                                          ▷ Return current minimum candidate solution.

```

The modified BO loop is clearly visible (lines 5 – 16), with the additions of the transformation of the observed data (lines 3, 6 – 7 and 10), determining the optimal length-scales (line 9), discarding of observations (line 11) and the maximization of the bounded acquisition function (line 12).

We can now identify the mechanisms through which the objectives of this paper are addressed, these objectives being to develop a trust region BO-based method that (i) is resistant to computational slowdown, (ii) is adaptable to non-stationary and ill-conditioned functions without kernel engineering, and (iii) exhibits good convergence characteristics. Firstly, using the greedy data discarding strategy defined in Sec. 3.3, the number of observations used to construct the local GP surrogate is kept relatively constant at each algorithm iteration. This avoids the computational slowdown of standard BO with more observations noted in Sec. 2.1. Secondly, the use of a local trust region based on the local length-scales of GP surrogate allows the algorithm to adapt to the local behaviour of a non-stationary objective function. The rotation of the trust region using the weighted principal components also allows the trust region to adapt to ill-conditioning of the objective function in arbitrary directions. Lastly, the use of a transformed representation of the observed data X' and Y' that is forced to be well-conditioned allows the LABCAT algorithm to converge much closer to a solution before encountering the numerical issues encountered by standard BO.

3.6. Illustrative example

To illustrate the behaviour of the LABCAT algorithm compared to other trust region BO algorithms, consider the optimization of the Rosenbrock function [53], a well-known test function with a narrow, banana-shaped valley leading towards the global optimum. The starting point for the optimization algorithm is chosen at the end of this valley, typically a very challenging starting point for most optimization algorithms.

Firstly, consider an alternative formulation of the LABCAT algorithm without the weighted principal component rotation from (34) given in Fig. 3 (a). This algorithm behaves similarly to other trust region BO algorithms, with the trust region moving along the valley and recentred on the new minimum candidates. However, the narrowness of the valley forces the trust region to shrink rapidly. Due to the constraint we have placed on the acquisition function that the objective function may only be evaluated at subsequent points *inside* this trust region, this contraction slows progress towards the optimum considerably.

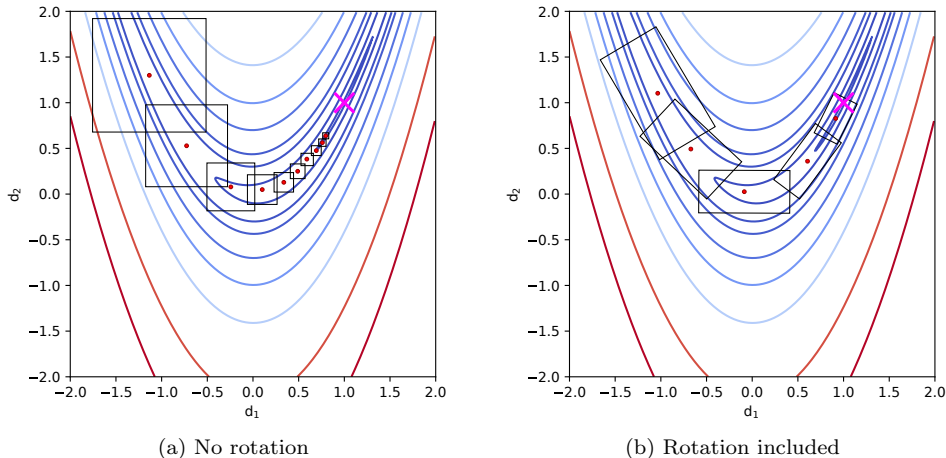


Figure 3: Illustrative example of the LABCAT algorithm applied to the 2-D Rosenbrock function (a) without and (b) with weighted principal component rotation. A subset of trust regions (indicated in black) centred on the respective minimum candidate solutions (indicated in red) are given and the global optimum is indicated by the magenta cross at $(1.0, 1.0)$. Only every fifth iteration is shown and observations other than the minimum candidate are not indicated to maintain visual clarity.

Next, consider the LABCAT algorithm with the aforementioned weighted principal rotation. Inspecting Fig. 3 (b), it is clear that this rotation yields a clear improvement. The rotation aligns the major axis of the rectangular trust region along the valley of the Rosenbrock function as the trust region moves through the valley. The trust region can now exploit the local separability of the valley by expanding and contracting along the major and minor axes of the trust region, by extension, the direction of the length-scales in the ARD kernel from (6). This version of the algorithm finds the optimum much faster than in Fig. 3 (a), demonstrating the value of the principal component rotation.

In the next section, numerical experiments on a wide suite of test functions are performed to obtain a general performance measure of the algorithm.

4. Experimental Results

With the proposed LABCAT algorithm, we present the results of a numerical performance analysis using computational experiments consisting of two sections. The first experiment compares the proposed LABCAT algorithm with similar trust region BO algorithms by applying them to several well-known, synthetic optimization test functions. The second experiment applies these algorithms, as well as algorithms from the wider field of derivative-free optimization, to the BBOB test suite using the COCO benchmarking software [36]. This extensive test suite is designed to be a representative sample of the more difficult problem distribution that can be expected in practical continuous-domain optimization. An ablation study is also

performed on the LABCAT algorithm using this benchmark to determine the contribution of each element of the algorithm to overall performance. Using the results from these benchmarks, we comment on the relative performance of LABCAT when compared to other algorithms and when applied to certain function groups with shared characteristics. All results in this report were obtained on a 11th generation Intel i7-11700 CPU @ 2.5 GHz, with the exception of those extracted from the COCO archive.

4.1. Synthetic test function benchmarks

In this section, we perform a comparison of the proposed LABCAT algorithm with standard BO and other trust region BO algorithms on selected, well-known 2-D test objective functions: the sphere (also known as the first De Jong function) [54], Branin-Hoo [55], Rosenbrock [53] (also known as the second De Jong function) and Levy [56] functions. These synthetic functions are each designed with certain properties and have been selected to cover a large variety of these problem properties. Both the sphere and Rosenbrock functions are unimodal, with the optimum of the Rosenbrock in a curved valley making convergence difficult. The Branin-Hoo and Levy functions are multimodal, with the Branin-Hoo function having several global minima and the Levy function having several local minima. The results in this section are, therefore, included for a comparison of the convergence behaviour between the proposed- and selected algorithms on a range of objective function characteristics.

LABCAT has been implemented using Rust and is available in the `labcat` library⁷. This library also provides a Python interface. For the other algorithms, we use the SRSM implementation from the Python `bayesian-optimization`⁸ library as well as the Python interfaces provided by the authors of the TuRBO, BADS and TREGO algorithms from the `turbo`⁹, `pybads`¹⁰ and `trieste`¹¹ libraries, respectively. A purely random search as well as standard BO, also from the `bayesian-optimization` package, is also included to serve as a performance baseline.

We run the LABCAT algorithm with a set of parameters within the recommended ranges ($\beta = 0.5, m = 7$ and $\sigma_{\text{prior}} = 0.1$) and the recommended DoE budget ($2d+1$) as described in Sec. 3.4. Each of the algorithms that we compared against is initialized with default parameters and a DoE budget of $2d+1$. The TuRBO algorithm is also used in two configurations: a single trust region (“TuRBO-1”) and five parallel trust regions (“TuRBO-5”). The results of this comparison is given in Fig. 4.

The noted shortcoming of standard BO, namely that BO struggles to converge to an arbitrary precision, is clearly visible. This deficiency is also inherited by the SRSM and TuRBO algorithms based on BO, clearly making very slow progress over 150 objective function samples. The BADS algorithm exhibits better convergence characteristics for the Branin-Hoo and Levy functions, possibly due to the deterministic mesh adaptive direct search (MADS) fallback step incorporated in this algorithm. It is clear that the LABCAT algorithm is not only capable of consistent convergence to a much higher level of precision for a wide range of objective function characteristics, but also may do so faster than comparable algorithms without needing to switch away from BO.

4.2. COCO black-box optimization benchmark

For the second experiment, we base our analysis on the comparing continuous optimizers (COCO) benchmarking software [36]. In this paper, we make use of the noiseless black-box optimization benchmarking (BBOB) test suite [37] that comprises 24 black-box objective functions to optimize. The functions in this test suite are collected into 5 groups, each with the following shared characteristics: (i) separable, (ii) unimodal with moderate conditioning, (iii) unimodal with high conditioning, (iv) multimodal with adequate global structure, and (v) multimodal with weak global structure.

To evaluate the performance of a single optimization algorithm on this suite, 15 *instances* of each function are generated, with each instance corresponding to a randomized modification of the function by a random

⁷<https://github.com/aemiliusRetiarius/LABCAT>

⁸<https://github.com/bayesian-optimization/BayesianOptimization>

⁹<https://github.com/uber-research/TuRBO>

¹⁰<https://github.com/acerbilab/pybads>

¹¹<https://github.com/secondmind-labs/trieste>

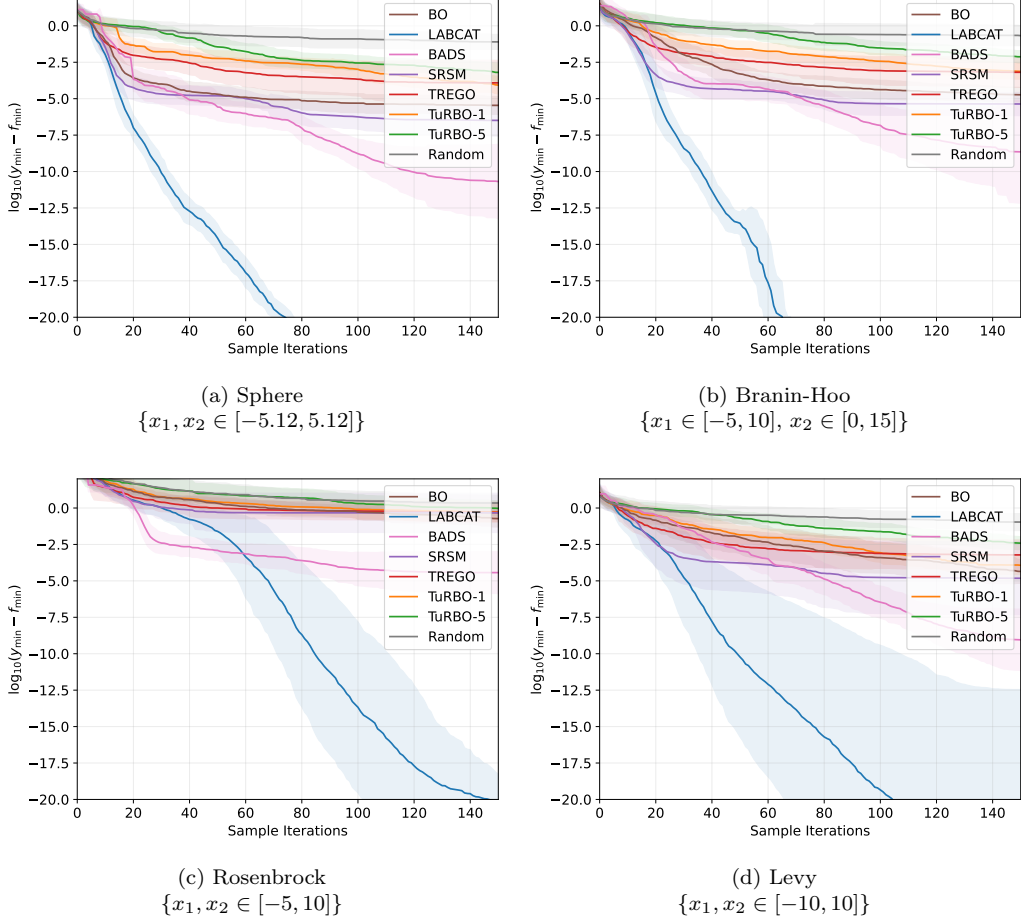


Figure 4: Performance of selected algorithms applied to synthetic 2-D test functions. We conduct 50 independent optimization runs per algorithm with a sampling budget of 150 objective function evaluations. The mean and standard deviation, indicated by the shaded regions, of the logarithmic global regret, which is the log-difference between the best candidate solution y_{\min} at each sampling iteration of the objective function and the global optimum f_{opt} , are reported. The domain of each objective function is also given in the respective subfigure captions.

translation of the optimum and a random rotation of the coordinate system. For each instance, an array of *problems* are also generated. Each of these problems are defined as a tuple comprising a function instance and a *target* precision to reach. To set these targets and give a good performance reference, COCO defines a composite algorithm known as *best2009*, an algorithm composed of the best performing optimization algorithm for each function from the BBOB-2009 workshop [57]¹². Similar to the experimental setup of Diouane et al. [32], we set the targets for each instance as the values reached by *best2009* after a certain number of objective function evaluations. Specifically, we set this number of function evaluations to a set of 50 values $[0.5, \dots, 100] \times d$, uniformly distributed in log-space. For the analysis in this paper, all of the algorithms tested are provided with a total sampling budget of $200d$ objective function evaluations per function instance to reach these targets. If an algorithm terminates before exhausting the sampling budget, unless otherwise specified, an independent restart is performed with the remaining sampling budget. With the results of an optimization algorithm applied to these problems, empirical cumulative distribution functions of runtimes

¹²Note that, due to being composed of the best performing algorithms for each function, outperforming *best2009* is quite a difficult task.

(runtime ECDFs) are compiled, which gives the proportion of problems solved by the algorithm for a given budget of objective function evaluations. Note that, similarly to the benchmarks in the previous section, a purely random search is also included in the analysis to serve as lower bound for performance. The results in this paper from the COCO software represent several weeks of combined CPU time on the previously mentioned hardware used in this paper.

4.2.1. LABCAT ablation study with the COCO benchmark

In this section, an ablation study is performed on the LABCAT algorithm to assess the contribution and significance of each component of the LABCAT algorithm on overall performance. The unablated algorithm is set the LABCAT algorithm with a set of parameters within the recommended ranges ($\beta = 0.5$, $m = 7$ and $\sigma_{\text{prior}} = 0.1$), denoted as “LABCAT”, and compared against instances of LABCAT with (a) no principal component rotation (“LABCAT noPC”), (b) more passive discarding of observations by doubling the maximum recommended value for m to 20 (“LABCAT m20”), (c) a uniform length-scale prior distribution (“LABCAT ULSP”), and (d) an increased number of or gradient steps during hyperparameter optimization (“LABCAT n10”). The results obtained by applying each of the ablated versions of LABCAT on the BBOB test suite is summarized in Fig. 5 and the full results are provided in Appendix E.1.

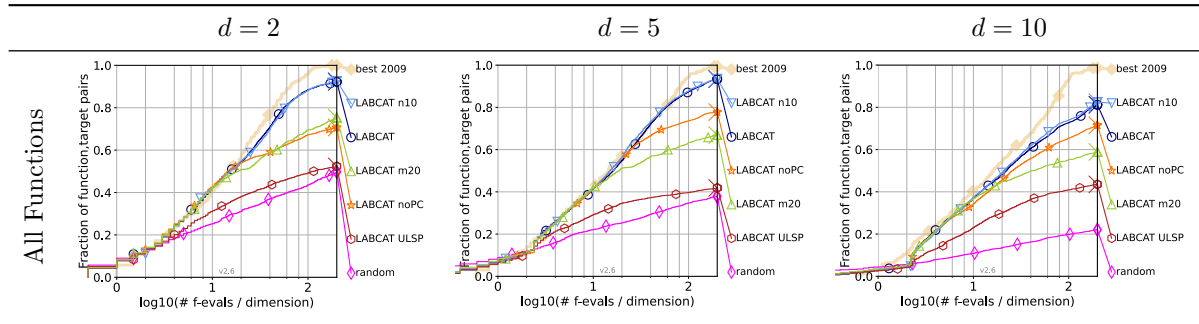


Figure 5: Selected empirical cumulative distribution functions (ECDFs) of runtimes table for ablation study with the COCO dataset over all functions in dimensions 2, 5 and 10. The values on the y -axis represent the proportion of runtime-based optimization targets achieved for a certain number of objective function samples. Algorithms that achieve these targets faster have a larger area under the curve and are therefore considered to have superior performance.

It is clear that the principal component rotation contributes significantly to the overall LABCAT algorithm performance, especially in lower dimensions and for unimodal functions in groups (ii) and (iii). This aligns with the behaviour observed in Sec. 3.6, as several of the functions in these groups are characterized by valleys with changes in direction similar to the Rosenbrock function. A similar contribution can be seen by the removal of observations, with a more pronounced difference in 5 and 10 dimensions. Severe performance degradation is observed when the Gaussian prior placed over the kernel length-scales in (40) is removed. While not indicated by the COCO-generated runtime ECDF graphs, a significant increase in the number of restarts was observed, indicating instability in the ablated LABCAT algorithm. As opposed to the previously mentioned modifications that may yield performance gains for certain function groups, removing the length-scale prior is a strict downgrade, with no performance gains in any function group. Additional or gradient steps during the optimization of the length scales yield little to no significant performance increases, therefore a single or gradient step seems to be sufficient, with all of the associated computational savings.

Inspecting Appendix E.1, it is interesting to note that removal of the principal component rotation and slower observation removal yields modest improvements when applied to the multimodal function groups (iv) and (v). This may be due to the slower convergence of these modified versions of the LABCAT algorithm leading to more exploration of the objective function space, finding slightly better solutions for these functions. In practice, if prior information regarding the objective function is available that indicates a multimodal structure and the additional computational cost can be spared, the observation cache multiplier m could be increased for better performance.

In summary, each of the constituent components of LABCAT contribute significantly to overall performance and the assumptions made in Sec. 3.2 and 3.3 are shown to be well founded.

4.2.2. Comparison with state-of-the-art optimization algorithms using the COCO benchmark

To compare the proposed LABCAT algorithm to similar algorithms from the wider field of derivative-free optimization, we expand the set of algorithms included in the comparison from Sec. 4.1 with the state-of-the-art DTS-CMA-ES, MCS, NEWUOA and SMAC algorithms. The DTS-CMA-ES [58] algorithm uses a surrogate-assisted evolution strategy based on a combination of the CMA-ES evolutionary algorithm and GP surrogates, known to be well-suited to multimodal problems. SMAC [3] is a variation of standard BO using an isotropic GP kernel and a locally biased stochastic search to optimize the EI. Multilevel coordinate search (MCS) [59] balances a global search based on the DIRECT [60] algorithm and a local search using a local quadratic interpolation. NEWUOA [61] also uses a quadratic interpolation, but combines it with a classical trust region approach.

Results for DTS-CMA-ES, MCS, NEWUOA and SMAC were obtained from the COCO database (see the respective publications [62, 63, 64, 65]). The results obtained by applying each of the functions on the BBOB test suite are shown on Fig. 6, with results in 2, 3 and 5 dimensions across all functions and from the selected function groups (iii) and (v). Complete results that include the other function groups can be found in Appendix E.2.

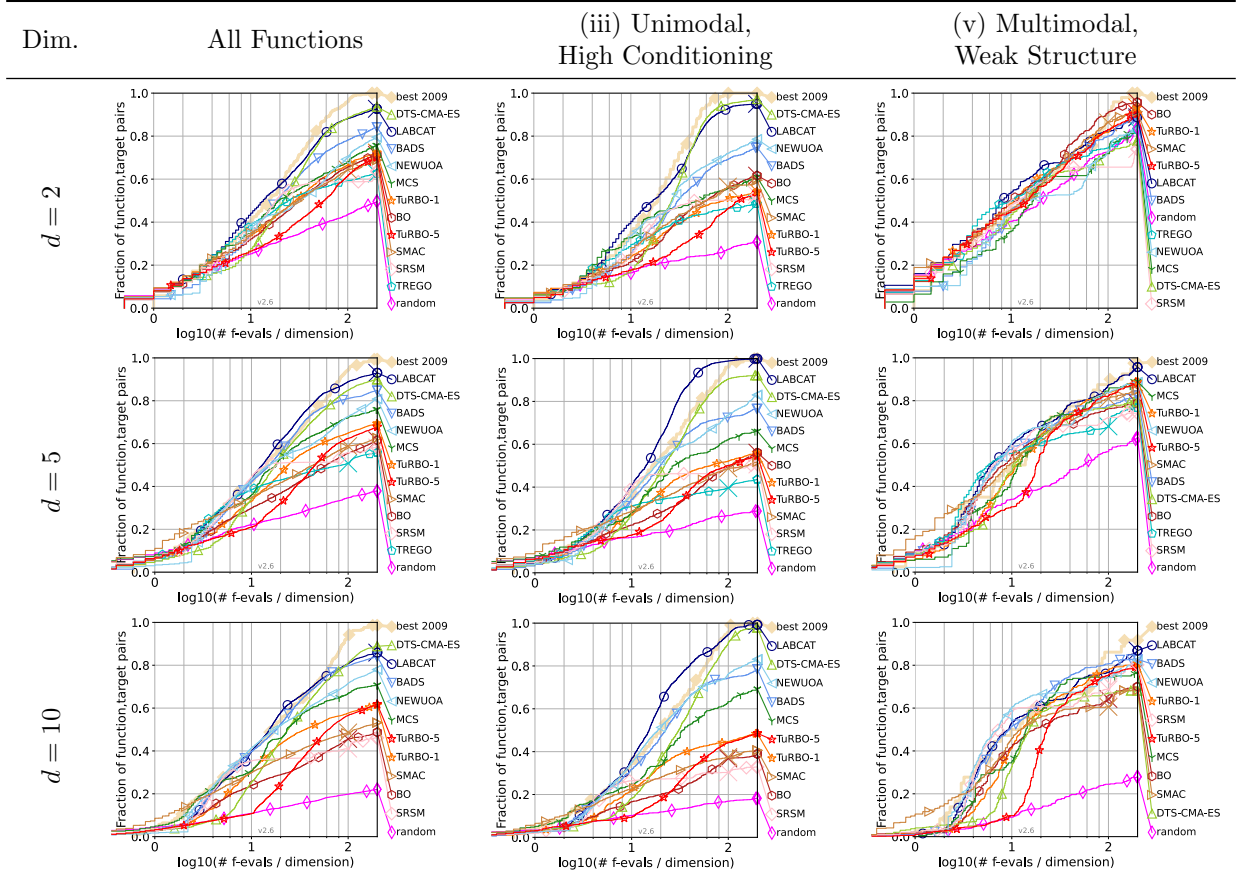


Figure 6: Selected empirical cumulative distribution functions (ECDFs) of runtimes table from the COCO dataset for comparison of the LABCAT algorithm with various state-of-the-art optimization algorithms in dimensions 2, 5 and 10. The first column reports the results of these algorithms applied to all 24 functions of the BBOB-2009 test suite for a given dimension while the second- and third columns report the results for the two most difficult function groups: (iii) unimodal functions with high conditioning (f10-f14) and (v) multimodal functions with weak global structure (f20-f24).

The results obtained from applying the selected algorithms to the COCO dataset reveal several important findings. Firstly, the LABCAT algorithm emerges as the top performer when considering the aggregate of all tested functions, having, from inspection, the largest area under the curve for any single algorithm in all dimensions (excluding the composite best2009 algorithm). Additionally, the algorithm excels particularly well when applied to unimodal functions with high conditioning from group (iii), even surpassing best2009 for a function group that is not traditionally considered to be well-suited for BO. Furthermore, the algorithm proves to be highly proficient for 2D and 5D, where it achieves the best performance of all of the BO-based algorithms, with a smaller performance gap in 10D between the LABCAT and BADS algorithms. Inspecting the results in Appendix E.2, the performance of the LABCAT algorithm is also slightly lower than those of other trust region BO algorithms (BADS, SRSM, TuRBO, TREGO) when applied to function group (iv), probably due to LABCAT heavily favouring local exploration of the objective function and, by extension, being unable to model the underlying global structure of these functions as well as the other algorithms.

The closest competitor from the trust region BO algorithms, when considering all functions, is the BADS algorithm. The BADS algorithm is, however, not very resistant to highly conditioned functions from group (iii), being consistently outperformed in this function group by the LABCAT algorithm. It is unclear how much of the performance of the BADS algorithm can be ascribed to its deterministic MADS fallback step, although some information may be gleaned by comparing this performance to another trust region BO method without this fallback step, such as TuRBO. In this comparison, similar performance is observed for multimodal functions, while BADS performs better for separable and unimodal functions. This may imply that the MADS algorithm incorporated into BADS allows for increased local exploitation when compared to other, “purer” trust region BO algorithms.

The only algorithm that approaches the performance of the LABCAT algorithm, and slightly outperforms it in 10D, for all functions is the DTS-CMA-ES algorithm. This algorithm ends essentially tied with LABCAT for 2D and slightly ahead in 10D once the sampling budgets have been exhausted, although the LABCAT algorithm still has a larger area under the curve in both of these cases. Although the DTS-CMA-ES algorithm exhibits a somewhat more sluggish start, it makes significant progress in subsequent iterations. From Appendix E.2, DTS-CMA-ES also performs noticeably better than the rest of the algorithms for multimodal functions with adequate global structure from group (iv), with this performance gap growing with dimension. This implies that DTS-CMA-ES is the algorithm that can leverage the underlying structure the most to ignore local minima.

Other observations of note include that SMAC seems to have an advantage for a very limited number of objective function evaluations before being overtaken, presumably due to SMAC being able to start optimizing before other algorithms have finished sampling their respective initial DoEs. The MCS algorithm also performs notably well for separable functions, possibly due to the deterministic nature of the search that is aligned with the separability axes.

In summary, the LABCAT algorithm is shown to be a leading contender in the field of expensive black-box function optimization, performing better, when considering all of the BBOB functions, than all of the considered BO-based methods, with the exception of being tied in 10D with the BADS algorithm.

5. Conclusions

Standard Bayesian optimization (BO) has several notable shortcomings, namely experiencing computational slowdown with additional algorithm iterations, not being well-suited to non-stationary and ill-conditioned functions, and exhibiting poor convergence characteristics. Trust region-based BO algorithms partially address these shortcomings by constraining the selection of the next point to be sampled from the objective function and incorporated into the Gaussian process (GP) surrogate model using an iteratively updated trust region. In this paper, we have constructed the LABCAT algorithm using two novel extensions of trust region-based BO. The first extension is an adaptive trust region- and objective function observation rescaling strategy, based on the length-scales of the local GP surrogate with an SE kernel and ARD, to allow for improved convergence characteristics. Secondly, this trust region is also rotated such that its axes are aligned with the weighted principal components of the observed data to allow the SE kernel with ARD to model non-stationary and ill-conditioned functions. Along with these extensions, the length-scales of the

ARD kernel are approximated iteratively and observed data outside of this trust region is greedily discarded to alleviate computational slowdown. An ablation study, using the extensive benchmark suite provided by the COCO software, is performed on the LABCAT algorithm which shows that each of the components of the LABCAT algorithm contribute significantly to the overall performance of the algorithm.

Using a set of diverse synthetic test functions, a comparison of the proposed LABCAT algorithm with standard BO and a variety of trust region-based BO algorithms shows that the LABCAT algorithm is capable of convergence to a much higher level of precision without encountering numerical issues or instability. A second comparison with a range of state-of-the-art black-box optimization methods from the wider field of black-box optimization, also performed using the aforementioned COCO benchmarking software, shows that the LABCAT algorithm is a leading contender in the domain of expensive black-box function optimization, significantly outperforming standard BO for nearly all tested scenarios and demonstrating exceptional performance compared to state-of-the-art black-box optimization methods, particularly in the domain of unimodal- and highly conditioned objective functions not typically associated with BO. This is coupled with a slight reduction in its effectiveness compared to other trust region-based BO methods when dealing with multimodal functions due to the increased emphasis of the LABCAT algorithm on local exploitation and a lack of a global surrogate model.

An important avenue for future work may include extending the LABCAT algorithm for use with a more general class of objective functions, such as modifying LABCAT to incorporate noisy output observations or categorical- and integer-valued input values (commonly encountered in the hyperparameters of machine learning models [66]) similarly to the kernel modification technique proposed by Garrido-Merchán and Hernández-Lobato [67]. The local GP model used in the LABCAT could also be augmented with gradient observations [12, Ch. 9] to improve the speed of the algorithm, possibly allowing for competitive performance when applied to non-black-box optimization problems.

CRediT authorship contribution statement

E. Visser: Conceptualization, Methodology, Software, Formal analysis, Writing - Original Draft, Writing - Review & Editing. **J.C. Schoeman:** Conceptualization, Writing - Review & Editing, Supervision. **C.E. van Daalen:** Conceptualization, Writing - Review & Editing, Supervision.

Declaration of competing interest

The authors declare that they have no known competing financial interests or personal relationships that could have appeared to influence the work reported in this paper.

Acknowledgements

This work was supported by grants from the Wilhelm Frank Bursary Fund as administered by Stellenbosch University from 2022 to 2023.

Appendix A. Offset proof

In the LABCAT algorithm, a transformed representation X' of the observed input set X is constructed according to the relation defined in (12)

$$\mathbf{X} = \mathbf{R}\mathbf{S}\mathbf{X}' + \mathbf{b}_x \mathbf{1}_n^\top \quad (\text{A.1})$$

During one of these transformations of X' , the current minimum of the centred input data \mathbf{x}'_{\min} is used to update the values of X' using the transform defined in (31)

$$\mathbf{X}'_{\text{new}} = \mathbf{X}' - \mathbf{x}'_{\min} \mathbf{1}_n^\top \quad (\text{A.2})$$

with the transformation parameter \mathbf{b}_x updated according to (21)

$$\mathbf{b}_{x_{\text{new}}} = \mathbf{b}_x + \mathbf{R}\mathbf{S}\mathbf{x}'_{\text{min}}. \quad (\text{A.3})$$

Substituting these new values into (A.1), using the fact that matrix multiplication is left- and right distributive, and simplifying yields

$$\begin{aligned} \mathbf{X} &= \mathbf{R}\mathbf{S}\mathbf{X}'_{\text{new}} + \mathbf{b}_{x_{\text{new}}}\mathbf{1}_n^\top \\ \mathbf{X} &= \mathbf{R}\mathbf{S}(\mathbf{X}' - \mathbf{x}'_{\text{min}}\mathbf{1}_n^\top) + (\mathbf{b}_x + \mathbf{R}\mathbf{S}\mathbf{x}'_{\text{min}})\mathbf{1}_n^\top \\ \mathbf{X} &= \mathbf{R}\mathbf{S}\mathbf{X}' + \mathbf{b}_x\mathbf{1}_n^\top - \mathbf{R}\mathbf{S}\mathbf{x}'_{\text{min}}\mathbf{1}_n^\top + \mathbf{R}\mathbf{S}\mathbf{x}'_{\text{min}}\mathbf{1}_n^\top \\ \mathbf{X} &= \mathbf{R}\mathbf{S}\mathbf{X}' + \mathbf{b}_x\mathbf{1}_n^\top. \end{aligned} \quad (\text{A.4})$$

Clearly, this implies that this is the same underlying mapping between X and X' from (A.1) expressed using the updated values of X' and \mathbf{b}_x , concluding the proof.

Appendix B. Weighted principal component alignment proof

In the LABCAT algorithm, a transformed representation X' of the observed input set X is constructed according to the relation defined in (12)

$$\mathbf{X} = \mathbf{R}\mathbf{S}\mathbf{X}' + \mathbf{b}_x\mathbf{1}_n^\top \quad (\text{B.1})$$

During one of these transformations of X' , the weighted principal components of the centred input data \mathbf{U}_a (33) is used to update the values of X' using the transform defined in (34)

$$\mathbf{X}'_{\text{new}} = \mathbf{S}^{-1}\mathbf{U}_a^\top \mathbf{S}\mathbf{X}' \quad (\text{B.2})$$

with the transformation parameter \mathbf{R} updated according to (25)

$$\mathbf{R}_{\text{new}} = \mathbf{R}\mathbf{U}. \quad (\text{B.3})$$

Substituting these new values into (B.1), recalling that the matrix \mathbf{U} obtained from the SVD is orthogonal ($\mathbf{U}^{-1} = \mathbf{U}^\top$), and simplifying yields

$$\begin{aligned} \mathbf{X} &= \mathbf{R}_{\text{new}}\mathbf{S}\mathbf{X}'_{\text{new}} + \mathbf{b}_x\mathbf{1}_n^\top \\ \mathbf{X} &= \mathbf{R}\mathbf{U}_a\mathbf{S}\mathbf{S}^{-1}\mathbf{U}_a^\top \mathbf{S}\mathbf{X}' + \mathbf{b}_x\mathbf{1}_n^\top \\ \mathbf{X} &= \mathbf{R}\mathbf{U}_a\mathbf{U}_a^\top \mathbf{S}\mathbf{X}' + \mathbf{b}_x\mathbf{1}_n^\top \\ \mathbf{X} &= \mathbf{R}\mathbf{S}\mathbf{X}' + \mathbf{b}_x\mathbf{1}_n^\top \end{aligned} \quad (\text{B.4})$$

Clearly, this implies that this is the same underlying mapping between X and X' from (B.1) expressed using the updated values of X' and \mathbf{R} , concluding the proof.

Appendix C. Rescaling proof

In the LABCAT algorithm, a transformed representation X' of the observed input set X is constructed according to the relation defined in (12)

$$\mathbf{X} = \mathbf{R}\mathbf{S}\mathbf{X}' + \mathbf{b}_x\mathbf{1}_n^\top \quad (\text{C.1})$$

During one of these transformations of X' , the most likely length-scales ℓ^* , collected into a diagonal matrix \mathbf{L}^{-1} from (27), is used to update the values of X' using the transform defined in (36)

$$\mathbf{X}'_{\text{new}} = \mathbf{L}^{-1} \mathbf{X}' \quad (\text{C.2})$$

with the transformation parameter \mathbf{S} updated according to (28)

$$\mathbf{S}_{\text{new}} = \mathbf{L} \mathbf{S} \quad (\text{C.3})$$

Both \mathbf{S} and \mathbf{L}^{-1} are diagonal scaling matrices. diagonal matrices are commutative

$$\begin{aligned} \mathbf{X} &= \mathbf{R} \mathbf{S}_{\text{new}} \mathbf{X}'_{\text{new}} + \mathbf{b}_x \mathbf{1}_n^\top \\ \mathbf{X} &= \mathbf{R} \mathbf{L} \mathbf{S} \mathbf{L}^{-1} \mathbf{X}' + \mathbf{b}_x \mathbf{1}_n^\top \\ \mathbf{X} &= \mathbf{R} \mathbf{S} \mathbf{L} \mathbf{L}^{-1} \mathbf{X}' + \mathbf{b}_x \mathbf{1}_n^\top \\ \mathbf{X} &= \mathbf{R} \mathbf{S} \mathbf{X}' + \mathbf{b}_x \mathbf{1}_n^\top \end{aligned} \quad (\text{C.4})$$

Clearly, this implies that this is the same underlying mapping between X and X' from (C.1) expressed using the updated values of X' and \mathbf{S} , concluding the proof.

Appendix D. Kernel matrix length-scale derivatives for squared exponential kernel with automatic relevance determination

During the optimization of the length-scales in Sec. 3.2, first- and second derivatives of the log-likelihood for GP fitted to the observations X' and Y' (10) with respect to the length-scales the length-scales of the squared exponential kernel function with automatic relevance determination (6) are calculated. These are defined by the Jacobian

$$\nabla \log p(Y' | X', \boldsymbol{\theta}) = \mathbf{J} := \left[\frac{\partial \log p(Y' | X', \boldsymbol{\theta})}{\partial \ln \ell_i} \right]_{1 \leq i \leq d} \quad (\text{D.1})$$

and the Hessian

$$\nabla^2 \log p(Y' | X', \boldsymbol{\theta}) = \mathbf{H} := \left[\frac{\partial^2 \log p(Y' | X', \boldsymbol{\theta})}{\partial \ln \ell_i \partial \ln \ell_j} \right]_{1 \leq i, j \leq d}.$$

Using the results derived in [45]¹³, the derivatives that define the entries of these matrices are given for the Jacobian

$$\frac{\partial \log p(Y' | X', \boldsymbol{\theta})}{\partial \ln \ell_i} = \frac{1}{2} \mathbf{y}'^\top \mathbf{K}^{-1} \frac{\partial \mathbf{K}}{\partial \ln \ell_i} \mathbf{K}^{-1} \mathbf{y}' - \frac{1}{2} \text{tr} \left(\mathbf{K}^{-1} \frac{\partial \mathbf{K}}{\partial \ln \ell_i} \right) \quad \forall i \in \{1, 2, \dots, d\} \quad (\text{D.2})$$

and Hessian

$$\begin{aligned} \frac{\partial^2 \log p(Y' | X', \boldsymbol{\theta})}{\partial \ln \ell_i \partial \ln \ell_j} &= \frac{1}{2} \text{tr} \left(\mathbf{K}^{-1} \frac{\partial^2 \mathbf{K}}{\partial \ln \ell_i \partial \ln \ell_j} \right) - \frac{1}{2} \text{tr} \left(\mathbf{K}^{-1} \frac{\partial \mathbf{K}}{\partial \ln \ell_j} \mathbf{K}^{-1} \frac{\partial \mathbf{K}}{\partial \ln \ell_i} \right) \\ &+ \mathbf{y}'^\top \mathbf{K}^{-1} \frac{\partial \mathbf{K}}{\partial \ln \ell_j} \mathbf{K}^{-1} \frac{\partial \mathbf{K}}{\partial \ln \ell_i} \mathbf{K}^{-1} \mathbf{y}' \\ &- \frac{1}{2} \mathbf{y}'^\top \mathbf{K}^{-1} \frac{\partial^2 \mathbf{K}}{\partial \ln \ell_i \partial \ln \ell_j} \mathbf{K}^{-1} \mathbf{y}' \quad \forall i, j \in \{1, 2, \dots, d\}. \end{aligned} \quad (\text{D.3})$$

¹³As stated in [45], directly calculating the matrix-matrix products in (38) and (39) should be avoided as far as possible. Instead, the products $\mathbf{K}^{-1} \frac{\partial \mathbf{K}}{\partial \ell_i}$ should be cached, matrix-vector products should be prioritised and only the products needed for the trace terms should be calculated.

These derivatives are specifically calculated with respect to the logarithm of the length-scales and achieved by transforming the derivatives of the kernel matrix \mathbf{K} (3) according to

$$\frac{\partial \mathbf{K}}{\partial \ln \ell_i} = \frac{\partial \mathbf{K}}{\partial \ell_i} \frac{\partial \ell_i}{\partial \ln \ell_i} \quad (\text{D.4})$$

to ensure that the length-scales are strictly positive. This transform is accomplished by multiplying the derivative of the length-scale with respect to its logarithm

$$\begin{aligned} \frac{\partial \ln \ell_i}{\partial \ell_i} &= \frac{1}{\ell_i} \\ \frac{\partial \ell_i}{\partial \ln \ell_i} &= \ell_i. \end{aligned} \quad (\text{D.5})$$

The kernel matrix derivative now becomes

$$\frac{\partial \mathbf{K}}{\partial \ln \ell_i} = \begin{bmatrix} \frac{\partial k(\mathbf{x}_1, \mathbf{x}_1)}{\partial \ln \ell_i} & \frac{\partial k(\mathbf{x}_1, \mathbf{x}_2)}{\partial \ln \ell_i} & \dots & \frac{\partial k(\mathbf{x}_1, \mathbf{x}_n)}{\partial \ln \ell_i} \\ \frac{\partial k(\mathbf{x}_2, \mathbf{x}_1)}{\partial \ln \ell_i} & \frac{\partial k(\mathbf{x}_2, \mathbf{x}_2)}{\partial \ln \ell_i} & \dots & \frac{\partial k(\mathbf{x}_2, \mathbf{x}_n)}{\partial \ln \ell_i} \\ \vdots & \vdots & \ddots & \vdots \\ \frac{\partial k(\mathbf{x}_n, \mathbf{x}_1)}{\partial \ln \ell_i} & \frac{\partial k(\mathbf{x}_n, \mathbf{x}_2)}{\partial \ln \ell_i} & \dots & \frac{\partial k(\mathbf{x}_n, \mathbf{x}_n)}{\partial \ln \ell_i} \end{bmatrix}. \quad (\text{D.6})$$

Note that the squared exponential kernel is symmetric (i.e. $k(\mathbf{x}_p, \mathbf{x}_q) = k(\mathbf{x}_q, \mathbf{x}_p)$), therefore the derivative of the kernel matrix is also symmetric

$$\frac{\partial \mathbf{K}}{\partial \ln \ell_i} = \left(\frac{\partial \mathbf{K}}{\partial \ln \ell_i} \right)^\top. \quad (\text{D.7})$$

In practical implementations, this symmetry allows the kernel matrix derivatives to be fully described by only calculating the upper- or lower triangular portions of the matrix.

Calculating the entries of (D.6) simply involve taking the derivative of (6) with respect to ℓ_i

$$\frac{\partial k(\mathbf{x}_p, \mathbf{x}_q)}{\partial \ell_i} = k(\mathbf{x}_p, \mathbf{x}_q) \cdot \frac{(x_{p_i} - x_{q_i})^2}{\ell_i^3} \quad (\text{D.8})$$

and multiplying with ℓ_i to obtain the derivative with respect to the logarithm of ℓ_i

$$\frac{\partial k(\mathbf{x}_p, \mathbf{x}_q)}{\partial \ln \ell_i} = \frac{\partial k(\mathbf{x}_p, \mathbf{x}_q)}{\partial \ell_i} \frac{\partial \ell_i}{\partial \ln \ell_i} = k(\mathbf{x}_p, \mathbf{x}_q) \cdot \frac{(x_{p_i} - x_{q_i})^2}{\ell_i^2}. \quad (\text{D.9})$$

Using these results, the second-derivative matrix with respect to the length-scales $\frac{\partial^2 \mathbf{K}}{\partial \ln \ell_i \partial \ln \ell_j}$ can be constructed. The entries of these matrices, in the case that $i \neq j$, is given as

$$\frac{\partial^2 k(\mathbf{x}_p, \mathbf{x}_q)}{\partial \ln \ell_j \partial \ln \ell_i} = \frac{\partial k(\mathbf{x}_p, \mathbf{x}_q)}{\partial \ln \ell_j} \cdot \frac{(x_{p_i} - x_{q_i})^2}{\ell_i^2}. \quad (\text{D.10})$$

Expanding and rearranging terms in this formula yields another symmetry

$$\begin{aligned}
\frac{\partial^2 k(\mathbf{x}_p, \mathbf{x}_q)}{\partial \ln \ell_j \partial \ln \ell_i} &= \frac{\partial k(\mathbf{x}_p, \mathbf{x}_q)}{\partial \ln \ell_j} \cdot \frac{(x_{p_i} - x_{q_i})^2}{\ell_i^2} \\
&= k(\mathbf{x}_p, \mathbf{x}_q) \cdot \frac{(x_{p_j} - x_{q_j})^2}{\ell_j^2} \cdot \frac{(x_{p_i} - x_{q_i})^2}{\ell_i^2} \\
&= k(\mathbf{x}_p, \mathbf{x}_q) \cdot \frac{(x_{p_i} - x_{q_i})^2}{\ell_i^2} \cdot \frac{(x_{p_j} - x_{q_j})^2}{\ell_j^2} \\
&= \frac{\partial k(\mathbf{x}_p, \mathbf{x}_q)}{\partial \ln \ell_i} \cdot \frac{(x_{p_j} - x_{q_j})^2}{\ell_j^2} \\
&= \frac{\partial^2 k(\mathbf{x}_p, \mathbf{x}_q)}{\partial \ln \ell_i \partial \ln \ell_j}.
\end{aligned} \tag{D.11}$$

This symmetry also implies the following symmetry in the log-likelihood Hessian matrix \mathbf{H} , reducing the calculations required to determine this matrix,

$$\frac{\partial^2 \mathbf{K}}{\partial \ln \ell_i \partial \ln \ell_j} = \left(\frac{\partial^2 \mathbf{K}}{\partial \ln \ell_i \partial \ln \ell_j} \right)^\top. \tag{D.12}$$

Lastly, for the case where $i = j$, i.e. the main diagonal of \mathbf{H} (39), the derivative is determined to be

$$\frac{\partial^2 k(\mathbf{x}_p, \mathbf{x}_q)}{\partial^2 \ln \ell_i} = \frac{\partial k(\mathbf{x}_p, \mathbf{x}_q)}{\partial \ln \ell_i} \left(\frac{(x_{p_i} - x_{q_i})^2}{\ell_i^2} - 2 \right). \tag{D.13}$$

Appendix E. COCO benchmark results

Appendix E.1. LABCAT ablation study COCO results

The full results of the LABCAT ablation study from Sec. 4.2.1 using the COCO benchmark are provided in this section.

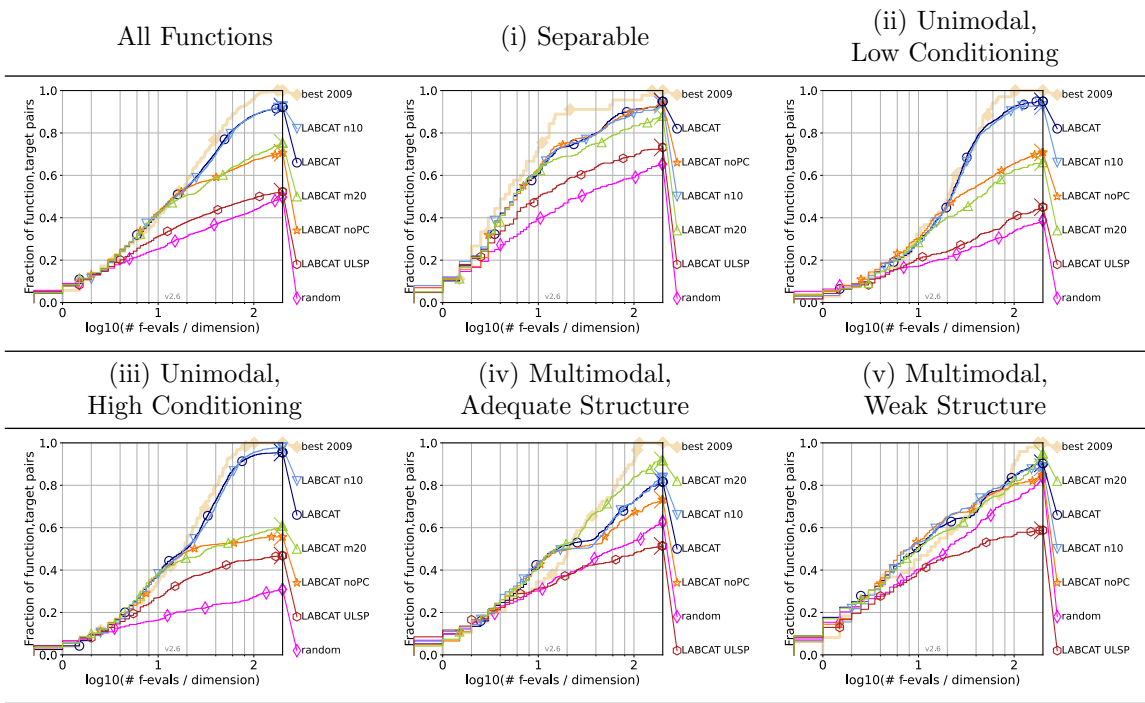


Figure E.1: 2D runtime ablation ECDFs table from COCO dataset

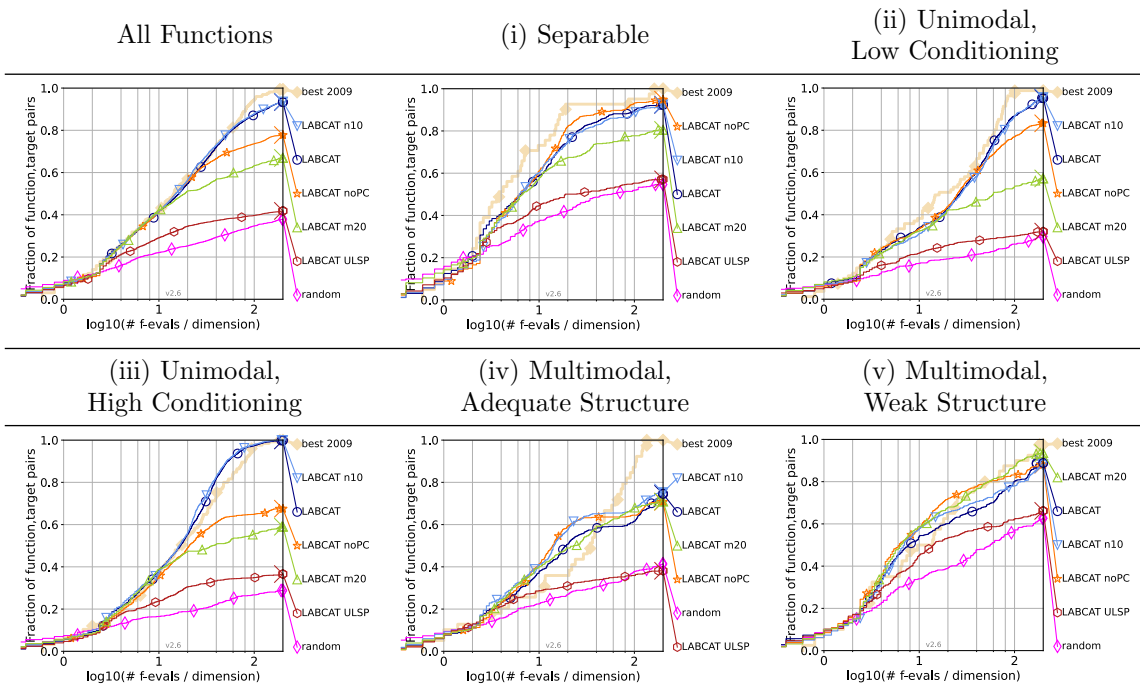


Figure E.2: 5D runtime ablation ECDFs table from COCO dataset

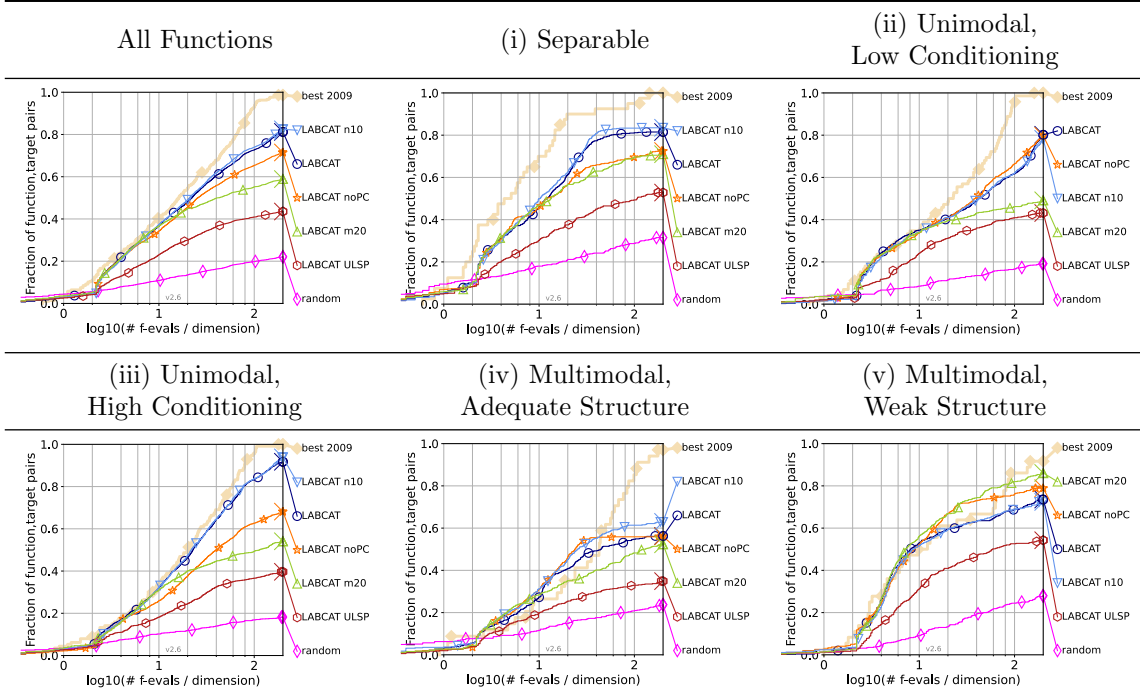


Figure E.3: 10D runtime ablation ECDFs table from COCO dataset

Appendix E.2. Full COCO results

The full results of the comparative algorithm study from Sec. 4.2.2 using the COCO benchmark are provided in this section.

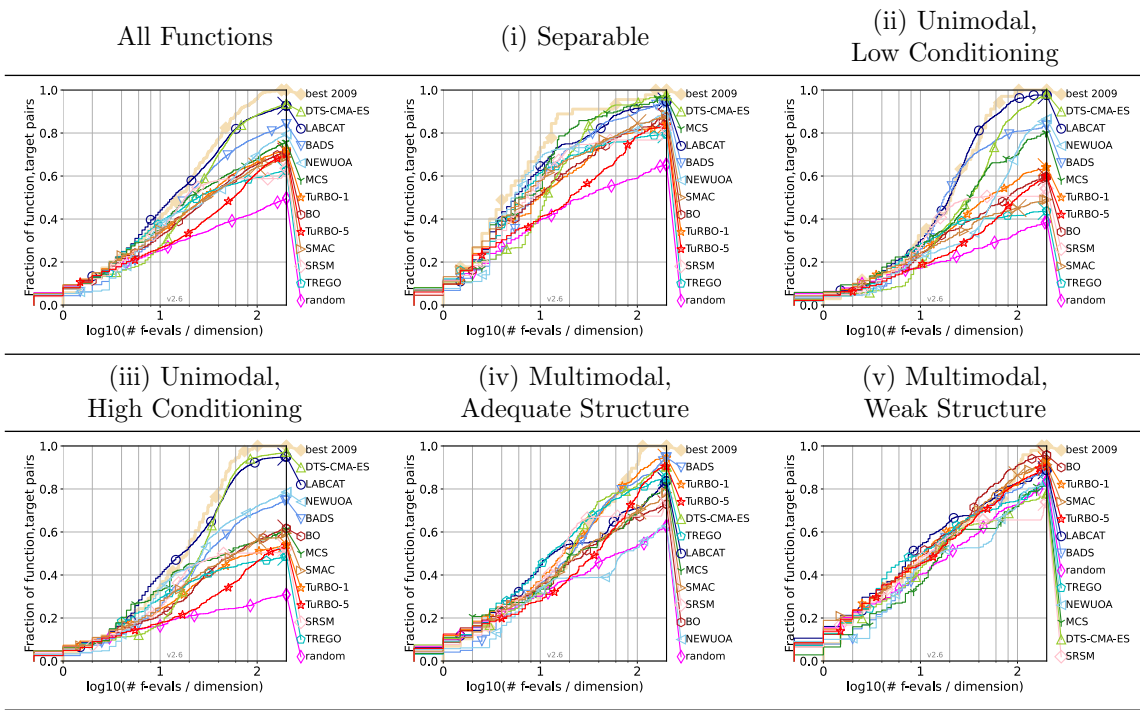


Figure E.4: 2D runtime ECDFs table from COCO dataset

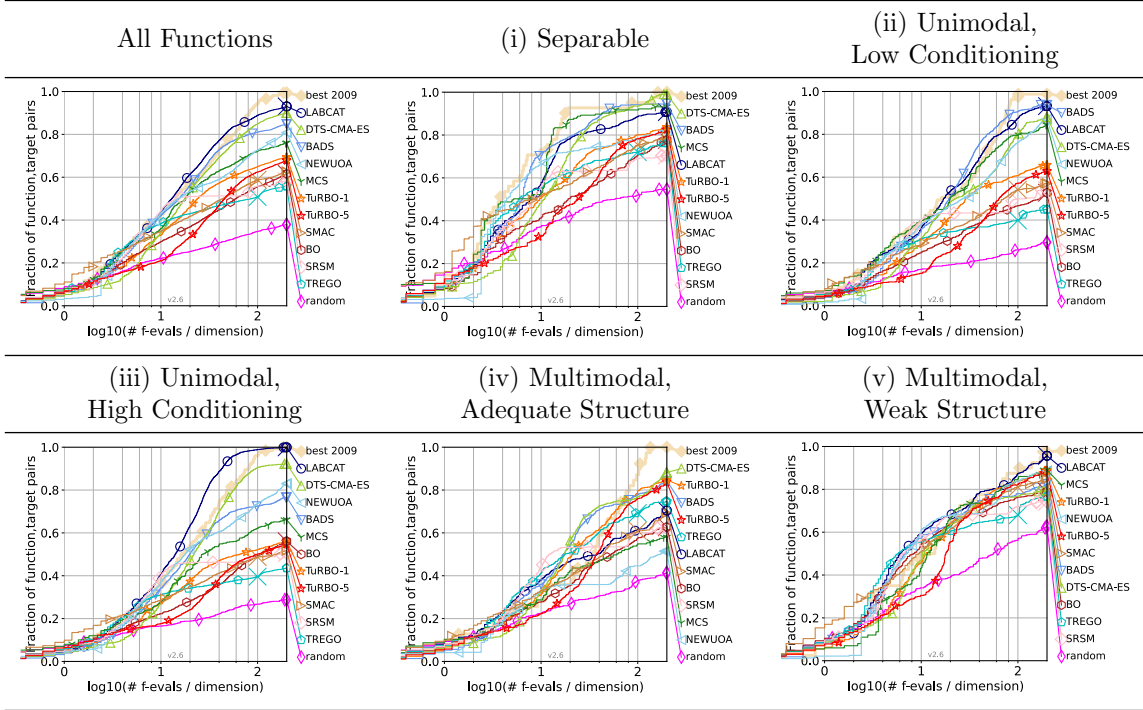


Figure E.5: 5D runtime ECDFs table from COCO dataset

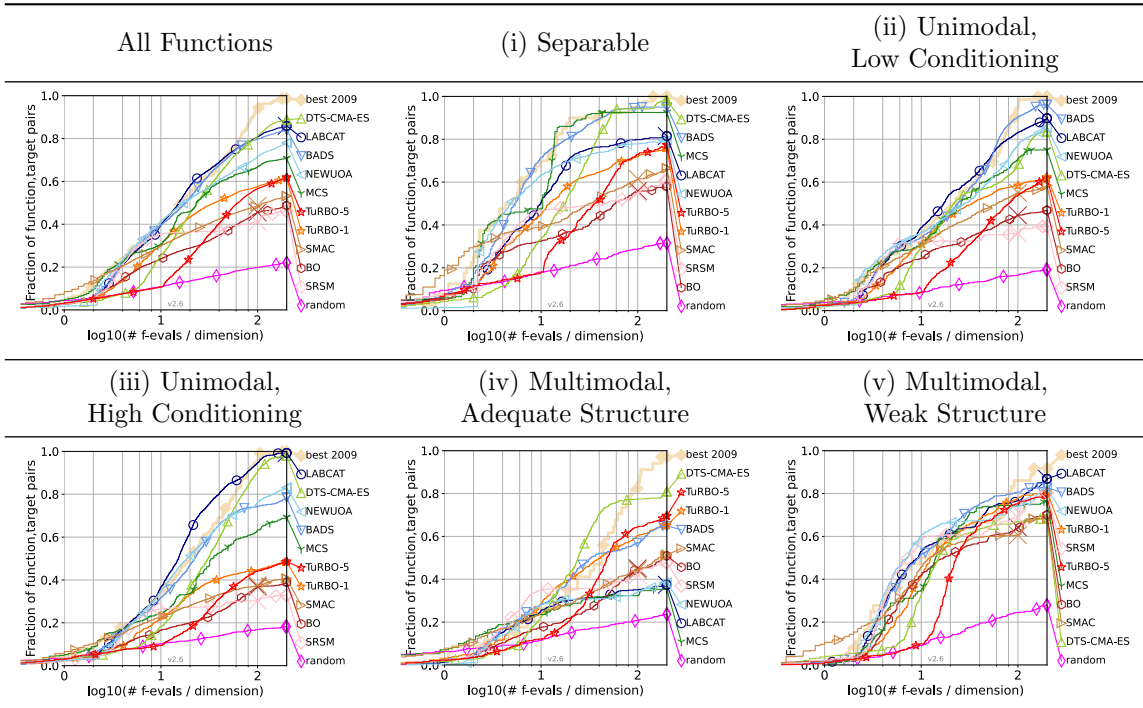


Figure E.6: 10D runtime ECDFs table from COCO dataset

References

- [1] D. R. Jones, M. Schonlau, W. J. Welch, Efficient global optimization of expensive black-box functions, *Journal of Global Optimization* 13 (1998) 455–492. [doi:10.1023/A:1008306431147](https://doi.org/10.1023/A:1008306431147).
- [2] D. Huang, T. Allen, W. Notz, N. Zeng, Global Optimization of Stochastic Black-Box Systems via Sequential Kriging Meta-Models, *Journal of Global Optimization* 34 (3) (2006) 441–466. [doi:10.1007/s10898-005-2454-3](https://doi.org/10.1007/s10898-005-2454-3).
- [3] F. Hutter, H. H. Hoos, K. Leyton-Brown, Sequential model-based optimization for general algorithm configuration, in: C. A. C. Coello (Ed.), *Learning and Intelligent Optimization*, Springer Berlin Heidelberg, Berlin, Heidelberg, 2011, pp. 507–523.
- [4] J. Bergstra, R. Bardenet, Y. Bengio, B. Kégl, Algorithms for hyper-parameter optimization, in: *Proceedings of the 24th International Conference on Neural Information Processing Systems*, NIPS’11, Curran Associates Inc., Red Hook, NY, USA, 2011, pp. 2546–2554.
- [5] D. Zhan, H. Xing, Expected improvement for expensive optimization: a review, *Journal of Global Optimization* (2020) 1–38.
- [6] T. Lai, H. Robbins, Asymptotically efficient adaptive allocation rules, *Advances in Applied Mathematics* 6 (1) (1985) 4–22. [doi:10.1016/0196-8858\(85\)90002-8](https://doi.org/10.1016/0196-8858(85)90002-8).
- [7] B. Shahriari, K. Swersky, Z. Wang, R. P. Adams, N. de Freitas, Taking the human out of the loop: A review of Bayesian optimization, *Proceedings of the IEEE* 104 (2016) 148–175.
- [8] J. Wu, X.-Y. Chen, H. Zhang, L.-D. Xiong, H. Lei, S.-H. Deng, Hyperparameter optimization for machine learning models based on Bayesian optimization, *Journal of Electronic Science and Technology* 17 (1) (2019) 26–40. <https://doi.org/10.11989/JEST.1674-862X.80904120>.
- [9] J. Snoek, H. Larochelle, R. P. Adams, Practical Bayesian optimization of machine learning algorithms, *Advances in neural information processing systems* 25 (2012).
- [10] R. Couperthwaite, A. Molkeri, D. Khatamsaz, A. Srivastava, D. Allaire, R. Arròyave, Materials design through batch Bayesian optimization with multisource information fusion, *JOM* 72 (12) (2020) 4431–4443. [doi:10.1007/s11837-020-04396-x](https://doi.org/10.1007/s11837-020-04396-x).
- [11] K. Wang, A. W. Dowling, Bayesian optimization for chemical products and functional materials, *Current Opinion in Chemical Engineering* 36 (2022) 100728. [doi:10.1016/j.coche.2021.100728](https://doi.org/10.1016/j.coche.2021.100728).
- [12] C. Rasmussen, C. Williams, *Gaussian Processes for Machine Learning*, Adaptive Computation and Machine Learning series, MIT Press, 2005. [doi:10.7551/mitpress/3206.001.0001](https://doi.org/10.7551/mitpress/3206.001.0001).
- [13] G. Lan, J. M. Tomczak, D. M. Roijers, A. Eiben, Time efficiency in optimization with a Bayesian-evolutionary algorithm, *Swarm and Evolutionary Computation* 69 (2022) 100970. [doi:10.1016/j.swevo.2021.100970](https://doi.org/10.1016/j.swevo.2021.100970).
- [14] J. Quiñonero-Candela, C. Rasmussen, C. Williams, O. Chapelle, D. Decoste, J. Weston, et al., *Approximation Methods for Gaussian Process Regression*. Large Scale Kernel Machines, MIT Press, 2007, Ch. 9, pp. 203–224.
- [15] R. Martinez-Cantin, Funneled Bayesian optimization for design, tuning and control of autonomous systems, *IEEE Transactions on Cybernetics* 49 (4) (2019) 1489–1500. [doi:10.1109/TCYB.2018.2805695](https://doi.org/10.1109/TCYB.2018.2805695).
- [16] R. G. Regis, C. A. Shoemaker, A quasi-multistart framework for global optimization of expensive functions using response surface models, *Journal of Global Optimization* 56 (4) (2013) 1719–1753. [doi:10.1007/s10898-012-9940-1](https://doi.org/10.1007/s10898-012-9940-1).
- [17] E. Vazquez, J. Bect, Convergence properties of the expected improvement algorithm with fixed mean and covariance functions, *Journal of Statistical Planning and Inference* 140 (11) (2010) 3088–3095. <https://doi.org/10.1016/j.jspi.2010.04.018>.
- [18] A. D. Bull, Convergence rates of efficient global optimization algorithms., *Journal of Machine Learning Research* 12 (10) (2011).
- [19] N. Srinivas, A. Krause, S. Kakade, M. Seeger, Gaussian process optimization in the bandit setting: No regret and experimental design, in: *Proceedings of the 27th International Conference on International Conference on Machine Learning*, ICML’10, Omnipress, Madison, WI, USA, 2010, pp. 1015–1022.
- [20] R. B. Gramacy, H. K. H. Lee, Cases for the nugget in modeling computer experiments, *Statistics and Computing* 22 (2010) 713–722.
- [21] T. Santner, B. Williams, W. Notz, *The Design and Analysis Computer Experiments*, Springer Series in Statistics, Springer, New York, NY, 2018. [doi:10.1007/978-1-4939-8847-1](https://doi.org/10.1007/978-1-4939-8847-1).
- [22] M. McLeod, S. Roberts, M. A. Osborne, Optimization, fast and slow: optimally switching between local and Bayesian optimization, in: *International Conference on Machine Learning*, PMLR, 2018, pp. 3443–3452.
- [23] P. P. Michael J. Sasena, P. Goovaerts, Exploration of metamodeling sampling criteria for constrained global optimization, *Engineering Optimization* 34 (3) (2002) 263–278. [doi:10.1080/03052150211751](https://doi.org/10.1080/03052150211751).
- [24] R. G. Regis, C. A. Shoemaker, Improved strategies for radial basis function methods for global optimization, *Journal of Global Optimization* 37 (1) (2007) 113–135. [doi:10.1007/s10898-006-9040-1](https://doi.org/10.1007/s10898-006-9040-1).
- [25] H. Mohammadi, R. Le Riche, E. Touboul, Making ego and cma-es complementary for global optimization, in: C. Dhaenens, L. Jourdan, M.-E. Marmion (Eds.), *Learning and Intelligent Optimization*, Springer International Publishing, Cham, 2015, pp. 287–292.
- [26] K. Kawaguchi, L. P. Kaelbling, T. Lozano-Perez, Bayesian optimization with exponential convergence, in: *Proceedings of the 28th International Conference on Neural Information Processing Systems - Volume 2*, NIPS’15, MIT Press, Cambridge, MA, USA, 2015, pp. 2809–2817.
- [27] Z. Wang, B. Shakibi, L. Jin, N. Freitas, Bayesian multi-scale optimistic optimization, in: *Artificial Intelligence and Statistics*, PMLR, 2014, pp. 1005–1014.

[28] K. P. Wabersich, M. Toussaint, Advancing Bayesian optimization: The mixed-global-local (MGL) kernel and length-scale cool down (2016). [arXiv:1612.03117](https://arxiv.org/abs/1612.03117).

[29] N. Stander, K. Craig, On the robustness of a simple domain reduction scheme for simulation-based optimization, *International Journal for Computer-Aided Engineering and Software (Eng. Comput.)* 19 (06 2002). [doi:10.1108/02644400210430190](https://doi.org/10.1108/02644400210430190).

[30] D. Eriksson, M. Pearce, J. R. Gardner, R. Turner, M. Poloczek, Scalable global optimization via local Bayesian optimization, in: *Proceedings of the 33rd International Conference on Neural Information Processing Systems*, Curran Associates Inc., Red Hook, NY, USA, 2019, pp. 5496–5507.

[31] L. Acerbi, W. J. Ma, Practical Bayesian optimization for model fitting with Bayesian adaptive direct search, *Advances in Neural Information Processing Systems* 30 (2017) 1834–1844.

[32] Y. Diouane, V. Picheny, R. L. Riche, A. S. D. Perrotolo, Trego: a trust-region framework for efficient global optimization, *Journal of Global Optimization* 86 (2021) 1–23.

[33] R. G. Regis, Trust regions in kriging-based optimization with expected improvement, *Engineering Optimization* 48 (6) (2016) 1037–1059. [doi:10.1080/0305215X.2015.1082350](https://doi.org/10.1080/0305215X.2015.1082350).

[34] Z. Zhou, Y. S. Ong, P. Nair, Hierarchical surrogate-assisted evolutionary optimization framework, in: *Proceedings of the 2004 Congress on Evolutionary Computation (IEEE Cat. No.04TH8753)*, Vol. 2, 2004, pp. 1586–1593 Vol.2. [doi:10.1109/CEC.2004.1331085](https://doi.org/10.1109/CEC.2004.1331085).

[35] R. M. Neal, *Bayesian Learning for Neural Networks*, Lecture Notes in Statistics, Springer, New York, NY, 1995. [doi:10.1007/978-1-4612-0745-0](https://doi.org/10.1007/978-1-4612-0745-0).

[36] N. Hansen, A. Auger, R. Ros, O. Mersmann, T. Tušar, D. Brockhoff, COCO: A platform for comparing continuous optimizers in a black-box setting, *Optimization Methods and Software* 36 (2021) 114–144. [doi:10.1080/10556788.2020.1808977](https://doi.org/10.1080/10556788.2020.1808977).

[37] N. Hansen, S. Finck, R. Ros, A. Auger, *Real-Parameter Black-Box Optimization Benchmarking 2009: Noiseless Functions Definitions*, Research Report RR-6829, INRIA (2009).

[38] R. A. Horn, C. R. Johnson, *Matrix Analysis*, 2nd Edition, Cambridge University Press, 2012. [doi:10.1017/CBO9781139020411](https://doi.org/10.1017/CBO9781139020411).

[39] J. Mercer, Functions of positive and negative type, and their connection with the theory of integral equations, *Philosophical Transactions of the Royal Society of London. Series A, Containing Papers of a Mathematical or Physical Character* 209 (1909) 415–446.

[40] R. H. Byrd, P. Lu, J. Nocedal, C. Zhu, A limited memory algorithm for bound constrained optimization, *SIAM J. Sci. Comput.* 16 (1995) 1190–1208.

[41] J. A. Nelder, R. Mead, A Simplex Method for Function Minimization, *The Computer Journal* 7 (4) (1965) 308–313. [doi:10.1093/comjnl/7.4.308](https://doi.org/10.1093/comjnl/7.4.308).

[42] H. Robbins, S. Monro, A stochastic approximation method, *The Annals of Mathematical Statistics* 22 (3) (1951) 400–407. [doi:10.1214/aoms/1177729586](https://doi.org/10.1214/aoms/1177729586).

[43] J. Han, M. Kamber, J. Pei, 3 - data preprocessing, in: J. Han, M. Kamber, J. Pei (Eds.), *Data Mining* (Third Edition), third edition Edition, The Morgan Kaufmann Series in Data Management Systems, Morgan Kaufmann, Boston, 2012, pp. 83–124. [doi:10.1016/B978-0-12-381479-1.00003-4](https://doi.org/10.1016/B978-0-12-381479-1.00003-4).

[44] G. W. Stewart, On the early history of the singular value decomposition, *SIAM Review* 35 (4) (1993) 551–566. [doi:10.1137/1035134](https://doi.org/10.1137/1035134).

[45] C. Moore, A. Chua, C. Berry, J. Gair, Fast methods for training Gaussian processes on large data sets, *Royal Society Open Science* 3 (May 2016). [doi:10.1098/rsos.160125](https://doi.org/10.1098/rsos.160125).

[46] M. Frean, P. Boyle, Using Gaussian processes to optimize expensive functions, in: W. Wobcke, M. Zhang (Eds.), *AI 2008: Advances in Artificial Intelligence*, Springer, Berlin, Heidelberg, 2008, pp. 258–267. [doi:10.1007/978-3-540-89378-3_25](https://doi.org/10.1007/978-3-540-89378-3_25).

[47] L. Armijo, Minimization of functions having Lipschitz continuous first partial derivatives., *Pacific Journal of Mathematics* 16 (1966) 1–3.

[48] P. I. Frazier, W. B. Powell, S. Dayanik, A knowledge-gradient policy for sequential information collection, *SIAM Journal on Control and Optimization* 47 (5) (2008) 2410–2439.

[49] P. Hennig, C. J. Schuler, Entropy search for information-efficient global optimization, *J. Mach. Learn. Res.* 13 (2012) 1809–1837.

[50] Y. Levitan, N. Markovich, S. Rozin, I. Sobol, On quasirandom sequences for numerical computations, *USSR Computational Mathematics and Mathematical Physics* 28 (3) (1988) 88–92. [doi:10.1016/0041-5553\(88\)90181-4](https://doi.org/10.1016/0041-5553(88)90181-4).

[51] F. Zhang, *The Schur complement and its applications*, Numerical Methods and Algorithms, Springer, 2005. [doi:10.1007/b105056](https://doi.org/10.1007/b105056).

[52] M. McKay, R. Beckman, W. Conover, A comparison of three methods for selecting values of input variables in the analysis of output from a computer code, *Technometrics* 21 (1979) 239–245. [doi:10.1080/00401706.1979.10489755](https://doi.org/10.1080/00401706.1979.10489755).

[53] H. H. Rosenbrock, An Automatic Method for Finding the Greatest or Least Value of a Function, *The Computer Journal* 3 (3) (1960) 175–184. [doi:10.1093/comjnl/3.3.175](https://doi.org/10.1093/comjnl/3.3.175).

[54] K. A. De Jong, An analysis of the behavior of a class of genetic adaptive systems, Ph.D. thesis, University of Michigan, USA (1975).

[55] F. H. Branin, Widely convergent method for finding multiple solutions of simultaneous nonlinear equations, *IBM Journal of Research and Development* 16 (5) (1972) 504–522. [doi:10.1147/rd.165.0504](https://doi.org/10.1147/rd.165.0504).

[56] M. Laguna, R. Martí, Experimental testing of advanced scatter search designs for global optimization of multimodal functions, *Journal of Global Optimization* 33 (2) (2005) 235–255. [doi:10.1007/s10898-004-1936-z](https://doi.org/10.1007/s10898-004-1936-z).

[57] N. Hansen, A. Auger, R. Ros, S. Finck, P. Pošek, Comparing results of 31 algorithms from the black-box optimiza-

tion benchmarking bboB-2009, in: Proceedings of the 12th Annual Conference Companion on Genetic and Evolutionary Computation, GECCO '10, Association for Computing Machinery, New York, NY, USA, 2010, pp. 1689–1696. doi:10.1145/1830761.1830790.

[58] L. Bajer, Z. Pitra, J. Repický, M. Holeňa, Gaussian Process Surrogate Models for the CMA Evolution Strategy, Evolutionary Computation 27 (4) (2019) 665–697. doi:10.1162/evco_a_00244.

[59] W. Huyer, A. Neumaier, Global optimization by multilevel coordinate search, Journal of Global Optimization 14 (4) (1999) 331–355. doi:10.1023/A:1008382309369.

[60] D. R. Jones, C. D. Perttunen, B. E. Stuckman, Lipschitzian optimization without the Lipschitz constant, Journal of Optimization Theory and Applications 79 (1) (1993) 157–181. doi:10.1007/BF00941892.

[61] M. J. D. Powell, The NEWUOA software for unconstrained optimization without derivatives, Springer US, Boston, MA, USA, 2006. doi:10.1007/0-387-30065-1_16.

[62] Z. Pitra, L. Bajer, J. Repický, M. Holeňa, Comparison of ordinal and metric Gaussian process regression as surrogate models for CMA evolution strategy, in: Proceedings of the Genetic and Evolutionary Computation Conference Companion, GECCO '17, Association for Computing Machinery, New York, NY, USA, 2017, pp. 1764–1771. doi:10.1145/3067695.3084206.

[63] W. Huyer, A. Neumaier, Benchmarking of MCS on the noiseless function testbed, unpublished manuscript on webpage at https://arnold-neumaier.at/ms/mcs_exact.pdf (2009).

[64] R. Ros, Benchmarking the NEWUOA on the BBOB-2009 function testbed, in: Proceedings of the 11th Annual Conference Companion on Genetic and Evolutionary Computation Conference: Late Breaking Papers, GECCO '09, Association for Computing Machinery, New York, NY, USA, 2009, pp. 2421–2428. doi:10.1145/1570256.1570338.

[65] F. Hutter, H. Hoos, K. Leyton-Brown, An evaluation of sequential model-based optimization for expensive blackbox functions, in: Proceedings of the 15th Annual Conference Companion on Genetic and Evolutionary Computation, GECCO '13 Companion, Association for Computing Machinery, New York, NY, USA, 2013, pp. 1209–1216. doi:10.1145/2464576.2501592.

[66] F. Pedregosa, G. Varoquaux, A. Gramfort, V. Michel, B. Thirion, O. Grisel, M. Blondel, P. Prettenhofer, R. Weiss, V. Dubourg, J. Vanderplas, A. Passos, D. Cournapeau, M. Brucher, M. Perrot, E. Duchesnay, Scikit-learn: Machine learning in Python, Journal of Machine Learning Research 12 (2011) 2825–2830.

[67] E. C. Garrido-Merchán, D. Hernández-Lobato, Dealing with categorical and integer-valued variables in Bayesian optimization with Gaussian processes, Neurocomput. 380 (C) (2020) 20–35. doi:10.1016/j.neucom.2019.11.004.